BDFLUX: A new bounded domain model for quantifying vertical streambed fluxes in streambeds using heat as a tracer

Wenguang Shi, Quanrong Wang, Maria Klepikova, Dylan J Irvine, Arwa Rashed, Zilong Liao

▶ **To cite this version:**

Wenguang Shi, Quanrong Wang, Maria Klepikova, Dylan J Irvine, Arwa Rashed, et al.. BDFLUX: A new bounded domain model for quantifying vertical streambed fluxes in streambeds using heat as a tracer. Journal of Hydrology, 2024, 633, pp.130981. 10.1016/j.jhydrol.2024.130981 . insu-04481414

HAL Id: insu-04481414
https://insu.hal.science/insu-04481414v1

Submitted on 28 Feb 2024

HAL is a multi-disciplinary open access archive for the deposit and dissemination of scientific research documents, whether they are published or not. The documents may come from teaching and research institutions in France or abroad, or from public or private research centers.

L'archive ouverte pluridisciplinaire **HAL**, est destinée au dépôt et à la diffusion de documents scientifiques de niveau recherche, publiés ou non, émanant des établissements d'enseignement et de recherche français ou étrangers, des laboratoires publics ou privés.

Journal Pre-proofs

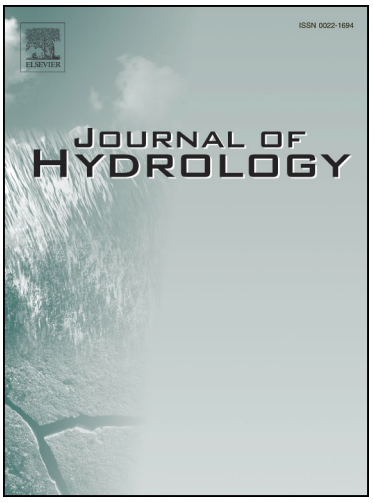

BDFLUX: A new bounded domain model for quantifying vertical streambed fluxes in streambeds using heat as a tracer

Wenguang Shi, Quanrong Wang, Maria Klepikova, Dylan J. Irvine, Arwa Rashed, Zilong Liao

PII: S0022-1694(24)00375-5
DOI: https://doi.org/10.1016/j.jhydrol.2024.130981
Reference: HYDROL 130981

To appear in: *Journal of Hydrology*

Please cite this article as: Shi, W., Wang, Q., Klepikova, M., Irvine, D.J., Rashed, A., Liao, Z., BDFLUX: A new bounded domain model for quantifying vertical streambed fluxes in streambeds using heat as a tracer, *Journal of Hydrology* (2024), doi: https://doi.org/10.1016/j.jhydrol.2024.130981

This is a PDF file of an article that has undergone enhancements after acceptance, such as the addition of a cover page and metadata, and formatting for readability, but it is not yet the definitive version of record. This version will undergo additional copyediting, typesetting and review before it is published in its final form, but we are providing this version to give early visibility of the article. Please note that, during the production process, errors may be discovered which could affect the content, and all legal disclaimers that apply to the journal pertain.

© 2024 Published by Elsevier B.V.

BDFLUX: A new bounded domain model for quantifying vertical streambed fluxes in streambeds using heat as a tracer

Wenguang Shi[1, 2, 3], Quanrong Wang[1, 3, 4, *], Maria Klepikova[2, *], Dylan J. Irvine[5, 6], Arwa Rashed[2], and Zilong Liao[1]

[1] Yinshanbeilu Grassland Eco-hydrology National Observation and Research Station, China Institute of Water Resources and Hydropower Research, Beijing 100038, PR China

[2] Univ Rennes, CNRS, Géosciences Rennes - UMR 6118, F-35000 Rennes, France

[3]School of Environmental Studies, China University of Geosciences, Wuhan 430078, PR China

[4] MOE Key Laboratory of Groundwater Quality and Health, China University of Geosciences, Wuhan 430078, PR China

[5] Research Institute for the Environment and Livelihoods, Charles Darwin University, Casuarina 0810, Australia.

[6] National Centre for Groundwater Research and Training, Bedford Park 5042, Australia.

Corresponding author: Quanrong Wang (wangqr@cug.edu.cn) and Maria Klepikova (maria.klepikova@univ-rennes1.fr).

Journal Pre-proofs

Journal Pre-proofs

28

Journal Pre-proofs

Highlights

- Heat-based bounded domain analytical model for vertical streambed flux presented.
- Particle swarm optimization and Markov Chain Monte Carlo methods used.
- Model is evaluated using synthetic, laboratory experimental, and field data.
- Method to estimate nonvertical flow components presented.

Journal Pre-proofs

Abstract

The use of heat as a tracer has become a widely used approach to estimate vertical streambed fluxes (VSFs). We present BDFLUX, a new bounded domain model that can be used as a rapid-screening tool to quantify VSFs and thermal properties of streambed sediments by analyzing on-site temperature-time series. BDFLUX uses a closed-form analytical solution that takes thermal advection and thermal conduction into account. BDFLUX, unlike other one-dimensional closed-form analytical solutions, does not assume an infinitely extending semi-infinite half-space. The initial and boundary conditions are described by arbitrary functions that can be directly determined by fitting the measured temperature-time series in the streambed at various depths. The particle swarm optimization (PSO) method and Markov Chain Monte Carlo (MCMC) method are used to estimate VSFs using temperature-time series observed at three depths. BDFLUX is validated using synthetic temperature-time series, demonstrating that it can perform well when the top and bottom boundary conditions are determined directly by the measured data. The capabilities of BDFLUX are further evaluated using laboratory and field data. The simulation results show that BDFLUX performed well in terms of interpreting laboratory experiments and field data, with a root mean square error as low as 0.059. The simulation of laboratory experiments shows that the MCMC method has a lower computational efficiency than PSO method. The magnitude of nonvertical flow components at a field site were quantified by analyzing the results of estimated VSFs in different vertical subdomains. Overall, BDFLUX improves one-dimensional heat analytical models in terms of assessing the magnitude of the nonvertical flow component in heterogeneous streambed sediments.

Keywords: Heat tracer method, Vertical streambed fluxes, Thermal conduction, Parameter estimation, Groundwater-surface water interaction.

Journal Pre-proofs

1. Introduction

Vertical streambed fluxes (VSFs) are critical for understanding surface water-groundwater interactions and impact biogeochemical processes in riparian zones (Chen et al., 2022a; Irvine et al., 2020; Rau et al., 2014). However, accurately determining VSFs is challenging due to their dynamic nature over time and space (Irvine et al., 2016; Irvine et al., 2015a; Keery et al., 2007), as well as the intricate three-dimensional flow fields involved (Banks et al., 2017; Irvine and Lautz, 2015; Reeves and Hatch, 2016). As evidenced by reviews of Anderson (2005), Constantz (2008), Rau et al. (2014), Abbott et al. (2016), and Tripathi et al. (2021), using heat as a natural tracer represents a powerful tool for determining VSFs and has many advantages over alternative methods such as geochemical tracer and hydraulic methods (Ren et al., 2018; Saar, 2011). For instance, compared to geochemical tracers, heat is inexpensive, ubiquitous, and easily measured *in situ* with a large number of loggers and probes available (Ghysels et al., 2021; van Kampen et al., 2022). VSFs and effective thermal diffusivity of streambed sediments can be estimated by fitting a heat transport model to temperature data collected from streambed sediments (Bredehoeft and Papaopulos, 1965; Hatch et al., 2006; Irvine et al., 2017;Stallman, 1965). The accuracy and robustness of parameter estimation from the abovementioned methods are heavily dependent on the reliability and performance of the chosen conceptual model, which must effectively represent to the physical processes of flow and heat transport.

A variety of analytical models in a semi-infinite domain have been developed to determine VSFs using temperature-time series collected within the stream and at different depths in the sediments of the streambed. Suzuki (1960) pioneered the use of streambed temperature measurements to estimate VSFs by developing an analytical solution to the one-dimensional (1D) vertical heat transport equation, where the upper boundary is represented by a sinusoidal temperature function, and the lower boundary is maintained at a constant temperature. Following the work of Suzuki (1960), three types of models were developed based on temperature measurements. The first type of models estimate VSFs using time-invariant temperature-depth profiles, such as Bredehoeft and Papaopulos (1965), Kurylyk et al. (2017), and Lin et al. (2022). The main limitation of these models is related to the challenges in estimating VSFs in the presence of varying surface temperatures. Irvine et al. (2020) showed that these limitations can be overcome using daily averaged temperatures, but that the approach can only be applied for groundwater discharge (upwards flow) conditions. The second type of models were developed to determine VSFs using temperature-time series measured at different depths within the streambed (Chen et al., 2018; Kurylyk and Irvine, 2016; Luce et al., 2017; . For example, by assuming heat transport in a semi-infinite domain streambed system, Shi and Wang (2023) recently developed a multi-layered heat transport model. However, as demonstrated by van Kampen et al. (2022) using synthetic and field data, this assumption can result in erroneous estimations of streambed fluxes. The use of MATLAB routines facilitates the application of the analytical models such as Hatch et al. (2006), Keery et al. (2007), McCallum et al. (2012) and Luce et al. (2013) in estimating VSFs in the streambed by using temperature signal characteristics like amplitude ratio and phase shift, such as VFLUX (Gordon et al., 2012) and VFLUX 2 (Irvine et al., 2015b). When using VFLUX 2, the shallow sensor pair outperforms the deep sensor pair due to the fast attenuation of temperature signals at streambed depths (Chen et al., 2018). All the above-mentioned analytical solutions are semi-infinite domain models. In comparison to these models, finite (bounded) domain models can offer significant advantages in terms of straightforward calculation and boundary conditions that more appropriately reflect real-world field conditions.

For example, the top and bottom boundary conditions can be directly determined from observed temperature-time series from different locations using a spline interpolation method, which is reliable, and it has been used to fit the top boundary condition and initial temperature distributions at various streambed depths in some semi-infinite domain models (Kurylyk and Irvine, 2016; Lin et al., 2022).

Unlike the analytical solutions mentioned above, models that use third type boundary conditions can apply frequency domain methods, which use spectral scaling factors of temperature-time series data in frequency domain to quantify VSFs (van Kampen et al., 2022; Schneidewind et al., 2016; Vandersteen et al., 2015). These models can divide the input temperature-time series data into noise, transient, and periodic components, as well as determine uncertainties of VSFs and streambed effective thermal diffusivity. These methods employ the local polynomial (LP) technique and maximum likelihood estimator (MLE) to address noise in input temperature-time series in the frequency domain, facilitating the estimation of VSFs and streambed effective thermal diffusivity. For example, the LPMLE model, which is coupled with LP and MLE, (Vandersteen et al., 2015) assumes heat transfer in a semi-infinite half-space, and requires two observations from different depths to estimate VSFs and streambed effective thermal diffusivity. Like the two types of methods mentioned above (i.e., Bredehoeft and Papaopulos (1965), and Hatch et al. (2006)), one important assumption contained in the LPMLE model is that heat transfer occurs in a semi-infinite half-space, where the lower boundary condition extends infinitely and is fixed at a constant temperature. Schneidewind et al. (2016) used local upper and lower boundary conditions to extend the LPMLE model to the LPMLE3 model to quantify VSFs and streambed thermal diffusivity. The LPMLE3 model is a bounded domain model, and it requires three observed points (at different depths) for each streambed subdomain of interest, where the observed points at the top and bottom of the streambed subdomain are worked as the boundary conditions, and the observed point inside the streambed subdomain is used for the estimation of VSFs and streambed effective thermal diffusivity. Recently, van Kampen et al. (2022) developed the LPMLEn model, which extends the capabilities of the LPMLE and LPMLE3 methods. This model facilitates the estimation of VSFs and streambed effective thermal diffusivity in bounded and infinite streambed domains, incorporating temperature measurements from n sensors in the parameter estimation process. The availability of advanced temperature sensors like fiber-optic distributed temperature sensing (DTS) (Selker et al., 2006; Vogt et al., 2010) or multilevel temperature lances (Munz et al., 2016) has made it straightforward to collect high spatial resolution temperature measurements.

The purpose of this study is to introduce BDFLUX, a new bounded domain model, that can be coupled with various inverse algorithms, like the particle swarm optimization (PSO) method or Markov Chain Monte Carlo (MCMC) methods, applied in the present study. BDFLUX is designed to solve an inverse problem by analyzing on-site temperature-time series, to extend the semi-infinite domain analytical models (Chen et al., 2018; Lin et al., 2022; Luce et al., 2013) to describe heat transport in a bounded (finite) streambed of interest (or streambed with layers). BDFLUX has three primary advantages over existing analytical methods: first, the BDFLUX can describe arbitrary initial conditions, arbitrary top and bottom boundary conditions based on temperature measurements in the finite streambed at various depths. Second, BDFLUX is simple to implement, and the VSFs, streambed effective thermal diffusivity and their uncertainties can be estimated simultaneously using a broad range of solver methods. BDFLUX is easily coupled with other parameter estimation methods such as the trial-and-error method (Chen et al., 2022b)

and iterative Levenberg-Marquardt method (Lin et al., 2022). Finally, it is more representative to quantify the VSFs for a bounded streambed or a layered streambed than to assume the streambed is homogeneous (van Kampen et al., 2022; Schneidewind et al., 2016; Vandersteen et al., 2015). Meanwhile, estimated VSFs in different vertical subdomains can be used to delineate the magnitude of nonvertical flow components. Compared to other 1D closed-form analytical models, BDFLUX does not assume an infinitely extending semi-infinite half-space with the lower boundary condition tending towards infinity. In contrast to LPMLE, LPMLE3 and LPMLEn methods, BDFLUX can handle arbitrary initial conditions based on temperature measurements at different depths within the finite streambed. The new analytical solution is specifically designed to solve an inverse problem by analyzing on-site temperature-time series. The capabilities of BDFLUX are tested using synthetic data, laboratory experimental data from Zhang et al. (2021), and field data from Ferencz et al. (2021).

2. Methodology

2.1 Mathematical model

The flow chart in Figure 1 depicts the process of estimating the VSFs and effective thermal diffusivity of a streambed using our newly developed analytical solution for heat transport in streambed materials. The workflow consists of three steps. First, developing a mathematical model of heat transport in a finite streambed with arbitrary initial and boundary conditions, which can be solved analytically using Green's function. The conceptual model is shown in Figure 1a. A cartesian coordinate system is used to develop the mathematical model, and the origin is located at the interface between the streambed and stream with the z-axis downward. The boundary conditions are described by arbitrary functions that can be directly determined by fitting the measured temperature-time series in the streambed at different depths. Second, the temperature-time series data collected from different depths of the streambed, as shown in Figure 1b, are used to estimate VSFs and thermal properties of streambed. BDFLUX, like the LPMLE3 and LPMLEn models, requires at least three observed points for a streambed subdomain of interest. For example, the four observation data sets in Figure 1a could be divided into two subdomains: subdomain 1 (SD1) for OBS1, OBS2, and OBS3, and subdomain 2 (SD2) for OBS2, OBS3, and OBS4. In the SD1, OBS1 and OBS3 are served as boundary conditions, whereas OBS2 is used for parameter estimation. Similarly, OBS2 and OBS4 are used as boundary conditions in the SD2, while OBS3 is used for parameter estimation. All four observations can also form a subdomain, where the middle two observations are used simultaneously for parameter estimation. Third, BDFLUX model, when combined with a broad range of solver methods like the PSO method, allows for the simultaneous estimation of VSFs and the effective thermal diffusivity for each streambed subdomain. Theoretically, if there is no nonvertical flow component in the streambed, the estimated VSFs are the same in SD1 and SD2. Otherwise, there will be a difference of the estimated VSFs between SD1 and SD2, where the differences in VSFs among distinct streambed subdomains indicates alterations in the magnitude of the nonvertical flow component.

The 1D advection-dispersion equation has been commonly used to describe heat transport processes in the streambed (e.g., Hatch et al., 2006; Luce et al., 2013; McCallum et al., 2012). The mathematical model of 1D vertical heat transport in a bounded domain with an arbitrary boundary and initial conditions is:

$$\frac{\partial T}{\partial t} = D\frac{\partial^2 T}{\partial z^2} - v\frac{\partial T}{\partial z},\ 0 \le z \le L,\ t > 0, \quad (1)$$

$$T(z, t = 0) = h(z),\ 0 \le z \le L,\ t > 0, \quad (2)$$

$$T(z = 0, t) = f(t),\ t > 0, \quad (3)$$

$$T(z = L, t) = g(t),\ t > 0, \quad (4)$$

where T is temperature [℃]; v is the thermal front velocity [m/d]; $h(z)$ is initial temperature distribution [℃]; $f(t)$ and $g(t)$ are arbitrary functions that describe the temperature [℃] at the top and bottom boundaries, respectively; t is time [d]; z is space [m]; L is the thicknesses [m] of streambed of interest; D is effective thermal diffusivity [$\mathrm{m^2/d}$].

For a saturated streambed, D and v can be described as (Chen et al., 2022b; Chen et al., 2018; Schneidewind et al., 2016):

$$D = \frac{k}{\rho c}, \quad (5)$$

$$k = k_s(1 - \theta) + \theta k_w, \quad (6)$$

$$v = \frac{\rho_w c_w}{\rho c} q, \quad (7)$$

$$\rho c = \theta \rho_w c_w + (1 - \theta)\rho_s c_s, \quad (8)$$

where k is thermal conductivity [$\mathrm{W/(m \cdot K)}$] of saturated streambed sediment; k_s and k_w are thermal conductivities [$\mathrm{W/(m \cdot K)}$] of solid and fluid phases, respectively, θ is porosity [-]; q is VSF [m/d], were a positive q indicates downwelling, and a negative q indicates upwelling; $\rho_w c_w$ and ρc are volumetric heat capacities [$\mathrm{J/(m^3 \cdot K)}$] of water and saturated streambed, respectively; $\rho_s c_s$ is specific volumetric heat capacity of the solids [$\mathrm{J/(m^3 \cdot K)}$]. ρ, ρ_w and ρ_s are densities [$\mathrm{kg/m^3}$] of the saturated streambed, water and solid, respectively; c, c_w and c_s are specific heat capacities [$\mathrm{J/(kg \cdot K)}$] of saturated streambed, water and solid, respectively. To account for thermal dispersion caused by flow velocity, some researchers include an additional thermal dispersivity term in Eq. (5) (Gossler et al., 2020; McCallum et al., 2012; Rau et al., 2012). However, thermal dispersivity will not be considered in this study because it becomes relatively minor and can be negligible when fluxes are small and over short spatial scales (Hatch et al., 2006; Luce et al., 2017; Schneidewind et al., 2016), especially when VSFs are slower than 10 m/d (Rau et al., 2012).

2.2 Closed-form solution

Eqs. (1) - (8) compose the 1D heat transport accounting for both conduction and advection in a bounded domain with an arbitrary boundary and initial conditions. The analytical solution for this model could be derived by applying Green's function method, which is easy to handle when arbitrary boundary and initial conditions are involved (Chen et al., 2018; Leij et al., 2000). This approach allows the top and bottom boundary conditions to be directly determined by interpolation (e.g., spline interpolation) from temperature-time series observed at different

locations. This method is reliable and has been successfully applied to simulate heat transport behavior in streambed sediments (Shi et al., 2023a; Shi et al., 2023b). Also, this method is unlike the models solved using the Laplace transform method, which requires a specific mathematical equation for the fitted function to be specified, for example, the models of Kurylyk and MacQuarrie (2014), Kurylyk and Irvine (2016), and Lin et al. (2022). The detailed solution derivation is provided in the supporting information, and the analytical solution is given as follows:

$$T = A(z,t)\left\{\int_0^L B(\lambda)G(z,t;\lambda,\tau=0)\,d\lambda + D\int_0^t [E(\tau)C(\tau) - H(\tau)F(\tau)]\,d\tau\right\}, \quad (9)$$

$$A(z,t) = exp\left[-\frac{v(vt-2z)}{4D}\right], \quad (10a)$$

$$B(\lambda) = h(\lambda)exp\left[-\frac{v\lambda}{2D}\right], \quad (10b)$$

$$C(\tau) = \sum_{n=1}^{\infty}\frac{2n\pi}{L^2}sin\left(\frac{n\pi z}{L}\right)exp\left[-D\left(\frac{n\pi}{L}\right)^2(t-\tau)\right], \quad (10c)$$

$$E(\tau) = f(\tau)exp\left[\frac{v^2\tau}{4D}\right], \quad (10d)$$

$$F(\tau) = \sum_{n=1}^{\infty}\frac{2n\pi}{L^2}(-1)^n sin\left(\frac{n\pi z}{L}\right)exp\left[-D\left(\frac{n\pi}{L}\right)^2(t-\tau)\right], \quad (10e)$$

$$G = \sum_{n=1}^{\infty}\frac{2}{L}sin\left(\frac{n\pi\lambda}{L}\right)sin\left(\frac{n\pi z}{L}\right)exp\left[-D\left(\frac{n\pi}{L}\right)^2(t-\tau)\right], \quad (10f)$$

$$H(\tau) = g(\tau)exp\left[\frac{v(v\tau-2L)}{4D}\right], \quad (10g)$$

where λ and τ refer to dummy variables, in which λ varies between 0 and L, τ varies between 0 and t, corresponding to the independent variables z and t, respectively.

Our model is an extension of previous 1D analytical models (Luce et al., 2013; McCallum et al., 2012; Stallman, 1965). For instance, if $L\to\infty$, $h(z) = T_0 + a_1 z + \delta exp(dz)$, $g(t) = T_0$, and $f(t)$ is a step functions of time, in which a_1, δ and d are coefficients, T_0 is subsurface temperature [℃] that is unaffected by surface temperature variation, the new model can be reduced to the model of Kurylyk and Irvine (2016). When $L\to\infty$, $g(t) = T_0$, $f(t)$ is described by a cosine function with an arbitrary amplitude, period, and phase shift, the present model can be reduced to the model of Chen et al. (2018).

2.3 Inverse modeling for VSFs estimation

We couple the present BDFLUX with the PSO method in order to search the optimal VSFs and D. Shi and Wang (2023) took a similar approach, using the PSO algorithm to estimate VSFs and streambed thermal characteristics in a multi-layered streambed system. The main advantages of PSO algorithm with respect to other inverse algorithms are: (1) PSO provides flexibility in estimating multiple parameters and enables efficient modification of the parameter count by

simply adjusting the initial settings without expanding the computations (Dya et al., 2021; Shi and Wang, 2023). (2) The PSO method converges rapidly by iteratively comparing the local and global extremum values, leading to a reduction in the number of iterations required. (3) It is simple to implement because it has been packaged into MATLAB (Ebbesen et al., 2012). Moreover, for comparison purposes, despite the high computational resources required for conducting MCMC simulations (Zhang et al., 2017), this study incorporates the application of the MCMC method in one of the laboratory experiments of Zhang et al. (2021). We used the method developed by Goodman and Weare (2010) as compared to traditional MCMC method, it can achieve much faster convergence, meanwhile, it is very simple to implement through using MATLAB code package "gwmcmc" (https://github.com/grinsted/gwmcmc).

2.4 Validation with numerical modelling

Two numerical models were developed in the COMSOL Multiphysics platform (COMSOL Inc., Burlington, MA, USA) to verify BDFLUX and to investigate the potential influence of bottom boundary condition on parameter estimation. The first numerical model, a 1D bounded domain model, was developed using the mathematical model of Eqs. (1) - (4) to verify BDFLUX. The model domain was 0.40 m long and was linearly discretized with a uniform spatial increment of 0.005 m ($dz = 0.005$ m), and a uniform time step of 0.01 d was used for simulation. The value of grid Péclet Number is less than 2 for the numerical simulations in this study, ensuring no numerical dispersion occurs. As observed temperature-depth profiles are not available and the temperature at a depth of 0.5 m is fluctuating around 28 ℃ (Figure 1b), the temperature at 0.5 m was taken as an initial temperature distribution $h(z)$. The top and bottom boundary conditions were taken from the measured data of Ferencz et al. (2021), namely, the measured temperature-time series at "OBS1" and "OBS3", as shown in Figure 1b, serve as top and bottom boundary conditions, respectively. More specifically, $f(t)$ and $g(t)$ were directly determined from observed temperature-time series at "OBS1" and "OBS3" using a spline interpolation method. The other model parameters are as follows: $k_s = 1.4$ W/(m · K), $k_w = 0.6$ W/(m · K), $c_s = 700$ J/(kg · K), $\rho_s = 2600$ kg/m^3, $\rho_w c_w = 4.20 \times 10^6$ J/(m^3 · K), $q = 0.1$ m/d, $L = 0.40$ m, and $\theta = 0.3$. These parameters, except q, were from the investigation of Ferencz et al. (2021). To access the simulation results, the root mean square error (RMSE) was employed, which can be calculated by:

$$RMSE = \sqrt{\frac{\sum_i^N \left(Y_i^{obs} - Y_i^{sim}\right)^2}{N}}, \tag{11}$$

where N is total number of the observations, Y_i^{obs} is true value (synthetic truth or observations) at time i, Y_i^{sim} is simulated value of the i^{th} realization at time i.

In many previous studies, the bottom boundary condition extended infinitely and was fixed at a constant temperature (Chen et al., 2022b; Lin et al., 2022; Rau et al., 2012). For the sake of comparison, a semi-infinite domain model was developed as the second numerical model to investigate the potential effects of bottom on parameter estimation. The semi-infinite domain ($0 \le z < \infty$) was replaced by a finite domain ($0 \le z < 10$ m). This assumption was validated through additional numerical testing on two different model domains ($0 \le z < 10$ m and $0 \le z < 500$ m) and the results shows a good agreement between both finite domains (see Figure

S1 in section S2 of supporting information for further information). This setup is reasonable because the diurnal temperature signals attenuate considerably in the streambed sediments approximately 0.5 meters below the surface (Kurylyk et al., 2019). In addition, like the treatment of Liang et al. (2019), a component within COMSOL known as an infinite element domain was used at $z = 10$ m to effectively represent the infinite boundary, this component employed rational coordinate scaling within a series of virtual domains that envelop the physical region. The model domain was linearly discretized with a uniform spatial step of 0.005 m. The initial and top boundary conditions, as well as the parameters used in the second numerical model, were the same as those used in the first numerical model, whereas the bottom boundary condition was set to 28 ℃.

To further validate the accuracy of BDFLUX in estimating q and D, the semi-infinite domain model with pre-defined input parameters was employed to produce temperature-time series at depths of 0.10, 0.20 and 0.30 m. The pre-defined parameter values are listed in Table 1. The BDFLUX model, coupled with PSO was then used to best-fit the synthetic temperature-time series to estimate the values of q and D simultaneously, in which the temperature-time series generated at depths of 0.1 and 0.3 m were worked as upper and lower boundary conditions, respectively, and the temperature-time series generated at depth of 0.2 m was used to parameter estimation. The accuracy of parameter estimation is evaluated using a relative error.

2.5 Validation with laboratory thermal tracer test data

The temperature-time series recorded from a laboratory column experiment reported by Zhang et al. (2021) were used to test the capabilities of BDFLUX. The sand column was constructed of Perspex pipe with a length of 0.45 m and an inner diameter of 0.075 m. The schematic representation of the laboratory experimental setup is shown in Figure 2 or in Figure 2 of Zhang et al. (2021). The sand column was uniformly filled with quartz sand with particle sizes ranging from 0.40 to 0.60 mm, with a measured total porosity of 0.45. Water in the supply tank is periodically heated and injected from the top of the sand column to produce a sinusoidal-like temperature input. Temperature-time series were measured at depths of 0.00, 0.10 and 0.20 m from the top of the filled media, and the filled media from the top to a depth of 0.20 m was considered a subdomain, as shown in Figure 2. Temperature-time series collected at depths of 0.00 and 0.20 m served as upper and lower boundary conditions, respectively, and temperature measurements recorded at depth of 0.10 m were used for estimating VSFs and effective thermal diffusivity. Downwelling flows were produced using two different q values (0.351 m/h and 0.199 m/h), which are denoted by Run1 and Run2 hereinafter. To simulate these data, we used a subordinated heat transport model (called Sub-HTE model) developed by Zhang et al. (2021) . The Sub-HTE model extended the classical 1D heat transport equation (HTE) by incorporating a time factor (α) to account for thermal retardation or storage resulting from hydro-biogeochemical processes. Although Zhang et al. (2021) developed the analytical solutions for the Sub-HTE model in the finite and semi-infinite domain scenarios, the lower boundary condition of the Sub-HTE model is assumed to be a constant. In addition, the Sub-THE model with a semi-infinite domain reduces to the HTE model when $\alpha = 1$. Note that the Sub-HTE model of Zhang et al. (2021) for simulation of the experiments of Run1 and Run2 is a bounded domain model. A more detailed information about these laboratory experiments can be found in Zhang et al. (2021). The best-fit values of thermal front velocity and effective thermal diffusivity for Run1 were 0.54

m/h and 1×10^{-4} m^2/h, respectively; and the corresponding best-fit values for thermal front velocity and effective thermal diffusivity in Run2 were 0.26 m/h and 1×10^{-4} m^2/h, respectively.

2.6 Application of BDFLUX using temperature-time series measured in Lower Colorado River

To test the field application of BDFLUX, temperature-time series data collected during 20-27 July 2017 at the Lower Colorado River, a dam-controlled fourth order river, as reported by Ferencz et al. (2021), are used in this study. The temperature-time series data were collected using purpose-built vertical temperature profilers. In each vertical temperature profiler, four thermistors were installed on an aluminum rod at 0.10, 0.20, 0.30, and 0.50 m intervals from the streambed. Most of the vertical flow is likely to occur at shallow depths beneath the center of the stream. In addition, using a 2D numerical simulation, Ferencz et al. (2021) found that the temperature distribution close to the river banks were dependent on advective heat transfer caused by hydrostatic fluctuations in river level, whereas the temperatures in the remaining part of the channel were primarily influenced by thermal conduction. Thus, two observations near the center of the river, denoted by VA1 and VA2 hereinafter, were chosen to reduce the effects of hydropeaking in this study. The majority of the streambed sediments in VA1 and VA2 are sand. Unlike the numerical model and sand column data, the Ferencz et al. (2021) dataset allows the application of BDFLUX to estimate the influence of non-vertical flows. To achieve this purpose, the four observed temperature-time series in each vertical temperature profiler could be divided into three subdomains: SDI for $z = 0.10$, 0.20 and 0.30 m,SDII for $z = 0.20$, 0.30 and 0.50 m, and SDIII for $z = 0.10$, 0.30 and 0.50 m. The SDIII is used to investigate the impact of the selected domain in BDFLUX on the estimation of VSFs by comparing it to the SDII results. The thermal properties of streambed sediment are the same as those used in Section 2.4.

3. Results and Discussions

3.1 Comparison of the present and numerical models in simulating temperature-time series

To verify the approaches used in BDFLUX, we used the numerical solution developed in Section 2.4 to produce temperature-time series at $z =$ 0.10, 0.20 and 0.30 m to compare with those generated by BDFLUX (Eqs. (6) - (7)). Figures 3a-3c show the comparison of temperature-time series between BDFLUX (green circle symbols) and the numerical solution (black solid curves) at $z =$ 0.10, 0.20 and 0.30 m, respectively. Figure 3 shows that the temperature-time series produced by the numerical solution are almost in agreement with those predicted by BDFLUX at given depths. All the $RMSE$ values between the BDFLUX and numerical solution are less than 0.0056. Figure 3 demonstrates that BDFLUX performs well when the top and bottom boundary conditions are determined directly by the measured data.

3.2 Comparison of the semi-infinite domain model with BDFLUX

The semi-infinite domain model developed in Section 2.4 is used to test the potential effects of bottom on heat transport in streambed. The temperature-time series are generated using the semi-infinite domain model and BDFLUX at depths of 0.10, 0.20 and 0.30 m. Figures 4a-4c show the comparison of BDFLUX and the semi-infinite domain model in terms of temperature-time series for $q =$ 0.01, 0.10 and 0.50 m/d, respectively. Two interesting observations can be

made from these results. First, the differences between these two models decrease as the VSFs increase, implying that the use of semi-infinite domain model may result in errors at low q. Second, although the top boundary condition is the same in these two models, the RSME values of temperature-time series increase as the depth of the observed locations increases (i.e., RSME values increase from 0.0193 to 0.3216 when $q = 0.10\ \mathrm{m/d}$), which is consistent with the findings of Zhang et al. (2021), who compared the capability of 1D bounded domain model (Sub-THE model with a finite domain) and semi-infinite domain model (THE model). Table 1 shows the estimated D and v values by BDFLUX with negligible error (i.e., all relative error levels less than 5%), indicating that BDFLUX can accurately estimate the D and v in a finite streambed domain. Further comparison of the BDFLUX with other bounded and semi-infinite domain models is shown in the Section 3.3.

3.3 Simulation results of laboratory experiments

In this section, the PSO method and MCMC method are employed to estimate v and D using the experimental data of Zhang et al. (2021) described in the section 2.5. The temperature-time series observed in the laboratory experiments at $z = 0.10$ m for Run1 ($q = 0.351\ \mathrm{m/h}$) and Run2 ($q = 0.199\ \mathrm{m/h}$) are displayed by green circle symbols in Figures 5a and 5b, respectively. The red solid curves and their corresponding 95 % confidence intervals are generated by BDFLUX using the estimated parameters obtained from the PSO method, in which the estimated parameters are listed in Table 2. For the sake of comparison, the simulation results of Zhang et al. (2021) are also included, where the "HTE model" and "Sub-HTE model" in the legend refer to the semi-infinite domain heat transport model and bounded domain heat transport model, respectively. Figure 5 shows that BDFLUX fits temperature-time series for both Run1 and Run2 slightly better than the two models of Zhang et al. (2021) mentioned above (i.e., RMSE of 0.059 compared to 0.354 and 0.366). As evidenced in Table 2, the thermal front velocities estimated by BDFLUX for both Run1 and Run2 are slightly lower than the models proposed by Zhang et al. (2021), whereas the estimated D by BDFLUX are close to three orders of magnitude higher than the values used in Zhang et al. (2021). It is worth noting that the effective D values for quartz sand estimated by the models of Zhang et al. (2021) may be lower than the true value. For example, Stonestrom and Constantz (2003) listed the thermal properties of various materials, including quartz, which has a thermal diffusivity of 0.0155 $\mathrm{m^2/h}$, a thermal conductivity of 8.4 $\mathrm{W/(m \cdot K)}$ and a specific volumetric heat capacity of $1.9 \times 10^6\ \mathrm{J/(m^3 \cdot K)}$. Based on the estimated thermal front velocities and effective thermal diffusivities by Zhang et al. (2021), we can further determine the thermal conductivity and volumetric heat capacity of quartz sand based on Eqs. (5) - (7), the estimated ρc, $\rho_s c_s$, k and k_s values by Sub-HTE and HTE models are listed in Table 3, where the values of θ and k_w used here for calculation are 0.45 and 0.60 $\mathrm{W/(m \cdot K)}$, respectively. As mentioned above, the estimated thermal conductivity values using the both Sub-HTE and HTE models of Zhang et al. (2021) are lower than those of organic matter (Stonestrom and Constantz (2003) reported the thermal conductivity of organic matter is 0.25 $\mathrm{W/(m \cdot K)}$), and the estimated thermal conductivity values using the Sub-HTE model are negative, which is physically unreasonable. According to Zhang et al. (2021), decreasing the best-fit fractional order (α) in the Sub-HTE model enhances thermal energy storage in the medium, that might explain the lower thermal conductivities estimated by the Sub-HTE model than the HTE model. Also, unlike BDFLUX, although the Sub-HTE model is a bounded domain model (the model

domain length is set to the length of the sand column), the lower boundary condition of the Sub-HTE model is treated as a constant like the HTE model.

As mentioned above, the D values estimated by BDFLUX are almost three orders of magnitude higher than the values used in Zhang et al. (2021), the likely reason is that the thermal dispersion processes occur due to the very high velocities q used during the two experiments (8.424 $\mathrm{m/d}$ for Run1 and 4.776 $\mathrm{m/d}$ for Run2). In order to calculate the potential thermal dispersion, we separated the D estimated by BDFLUX into two parts, the first one is thermal diffusivity and the second one is thermal dispersion, which can be described as (De Marsily, 1986; Rau et al., 2014):

$$D = \frac{k}{\rho c} + \beta \frac{\rho_w c_w}{\rho c} q, \tag{12}$$

where β is thermal dispersivity [m]. In this section, BDFLUX coupled with the PSO method was used to search the optimal parameters of k_s, $\rho_s c_s$, θ, and β. Porosity is also used as an objective parameter for optimization because the Run1 and Run2 were carried out in two different sand columns with potentially different porosities. For comparison, we also searched for parameter values of k_s, $\rho_s c_s$, and θ without β. The estimated results are listed in Table 3, in which D and v are also calculated based on the estimated results. When the optimal parameters are k_s, $\rho_s c_s$, and θ, the estimated thermal conductivity values for Run1 and Run2 using BDFLUX are 22.071 and 12.439 $\mathrm{W/(m \cdot ℃)}$, which are obviously physically unreasonable. In addition, the porosity values also seem to be underestimated. In contrast, when the optimal parameters are k_s, $\rho_s c_s$, θ and β, the estimated thermal conductivity values for Run 1 and Run 2 are close to the reference value in the literature of Stonestrom and Constantz (2003), and the estimated porosities for Run1 and Run2 are 0.4514 and 0.3856, respectively, in which the estimated porosity for Run1 closely matching the measured value. Although the same medium was used in both Runs 1 and 2, the estimated thermal property parameters ($k_s$and $\rho_s c_s$) are different. One probable explanation is that when the number of optimization parameters increases, the PSO method falls into a local optimum due to the inclusion of stochastic processes (Pallero et al., 2018). Comparing Table 2, however, we can find that using BDFLUX-optimized search parameters k_s, $\rho_s c_s$, θ, and β yields estimated D and v values that are remarkably close to the results obtained by only optimizing for D and v, especially for Run1. Finally, the estimated thermal dispersivity values of Run1 and Run2 are 0.0291 and 0.0181 m, respectively, as shown in Table 3. The estimated thermal dispersivity values are physically reasonable and are consistent with previous field studies (Keery et al., 2007; Rau et al., 2010; Ronan et al., 1998). As a result, we can infer that the thermal dispersion occurs in these two experiments.

Figures 6a and 6b show the frequency histograms of the v and D estimated by the MCMC method using temperature-time series collected from experiment of Run1, respectively. The simulation results of PSO method (red solid curve) and the model of Zhang et al. (2021) (magenta solid curve) are also included for comparison. The posterior distributions of v and D are close to normal while exhibiting fluctuations, and the posterior distribution of D fluctuates more significantly, suggesting that the uncertainty of D is larger, potentially due to thermal dispersivity. Figure 6c displays the comparison between the measured data and predicted temperature-time series generated by BDFLUX using the parameter samples from MCMC. The simulation results of PSO method (Figure 5a) are also included for comparison. It is important to

note that, although only a portion of the observations presented in Figure 6c were chosen for parameter estimation, the MCMC method took over 24 hours to yield the results presented (We used a standard desktop PC with a 6-core 2.60 GHz processor and 16.0 GB RAM). However, the PSO utilized all the observations and took only 36 minutes. Considering that MCMC has a low computational efficiency, it is not used for parameter estimation in the following sections. Similarly, the same observations can be found in Run2, as shown in Figure 7.

3.4 Simulation results of field tests in the Lower Colorado River

Quantification of VSFs across streambeds has become essential in the investigation of the transport and fate of contaminants and nutrients, ecological habitat, the management of water resources, and biochemical processes (Ghysels et al., 2021; Rau et al., 2014; Tripathi et al., 2021). Here, BDFLUX coupled with the PSO method was employed to estimate VSFs and D of streambed profile VA1 and streambed profile VA2 at two different depths based on the observed temperature-time series in the Lower Colorado River, which were divided into two subdomains as detailed in Section 2.6. The differences in VSFs between subdomains SDI and SDII were used to analyze the magnitude of potential nonvertical flow components, and the differences in VSFs between subdomains SDII and SDIII were employed to evaluate the impact of the selected domain in BDFLUX on the estimation of VSFs. Figures 8a to 8c show that the fitting of the temperature-time series (green circle symbols) observed in streambed profile VA1 by the proposed BDFLUX (red solid curves) for SDI, SDII, and SDIII, respectively. The estimated D of SDI, SDII and SDIII in streambed profile VA1 are 0.0798, 0.0790 and 0.0792 $\mathrm{m^2/d}$, respectively, and the estimated VSFs are 0.0347 $\mathrm{m/d}$ for SDI, 0.0333 $\mathrm{m/d}$ for SDII, and 0.0341 $\mathrm{m/d}$ for SDIII. Similarly, Figures 9a to 9c show that the fitting of the temperature-time series observed at streambed profile VA2 by BDFLUX for SDI, SDII and SDIII, respectively. The estimated D of SDI, SDII, and SDIII in streambed VA2 are 0.1034, 0.1018 and 0.1022 $\mathrm{m^2/d}$, respectively, and the estimated VSFs are -0.0090 $\mathrm{m/d}$ for SDI,-0.0769 $\mathrm{m/d}$ for SDII, and -0.0738 $\mathrm{m/d}$ for SDIII. The estimated D of SDI and SDII differs slightly for each streambed profile (VA1 and VA2). This is reasonable because the distance between SDI and SDII is relatively short, inferring that the streambed sediments are more likely to of similar materials. As for the estimated VSFs, those in streambed profile VA1 are downwelling and the magnitude of nonvertical flow components in streambed profile VA1 is 0.0014 $\mathrm{m/d}$, as shown in Figure 10a. The estimated VSFs in streambed profile VA2 are upwelling and the magnitude of nonvertical flow components in streambed profile VA2 is 0.0679 $\mathrm{m/d}$, as shown in Figure 10b. Note that the direction of the nonvertical flow component cannot be determined. The VSF estimated in SDIII is less than that estimated in SDII for both VA1 and VA2, which is most likely due to the presence of nonvertical flow between the depths of 0.1 and 0.2 m. In theory, the estimated VSF in SDII should be consistent with that of SDIII when there is no nonvertical flow component.

Moreover, by selecting shorter intervals of interest from the collected temperature-time series, BDFLUX coupled with the PSO method also allows for the estimation of time-variant VSFs and D. For example, the 5.75-day temperature-time series of SDI collected at VA1 (Figure 8a) was divided into 79 segments (the time interval is ~100 min), BDFLUX then estimated VSF and D within each time interval (the results are shown in Figure S2 of supporting information). The estimated VSF and D values using the entire dataset (5.75 days) are slightly higher than those estimated using the shorter time intervals. For comparison, the river stage observed by Ferencz et al. (2021) is also included, and the result shows that, although variations in estimated

VSF appear to be associated with river stage, the estimations have different degrees of fluctuation. This phenomenon is consistent with the findings of Shi et al. (2023a).

3.5 Limitations of BDFLUX

Compared to existing analytical solutions to the 1D heat transport models, BDFLUX can handle arbitrary initial and boundary conditions based on temperature measurements at different depths within the finite streambed, and BDFLUX does not assume an infinitely extending semi-infinite half-space with the lower boundary condition tending towards infinity. BDFLUX, like previous heat tracer approaches, has the following limitations.

(1) The BDFLUX approach considers the subsurface to be a homogeneous, finite domain with hydraulic and thermal characteristics that are assumed constant within the model domain. However, these assumptions can be violated in natural settings, particularly with the existence of significant heterogeneity (Irvine et al., 2016; Irvine et al., 2015a; Klepikova et al., 2016). Also, the BDFLUX approach can not consider the temperature dependency of viscosity and density. To date, these effects can only be investigated using numerical models, such as Lautz (2010) and Klepikova et al. (2016).

(2) As demonstrated in Section 3.4, although BDFLUX can infer the magnitude of nonvertical flow components, the direction of the nonvertical flow component cannot be predicted accurately. In addition, the estimation of VSF is subject to uncertainties associated with sensor precision, sensor actual depth, and surface temperature variations due to weather change (Irvine et al., 2016).

(3) BDFLUX approach cannot consider the temperature difference between the fluid and adjacent solid phases in saturated streambed sediment, i.e., the local thermal nonequilibrium effects. Previous investigations have highlighted that local thermal nonequilibrium effects are expected to be strong in fast flowing gravel media (Baek et al., 2022; Gossler et al., 2020; Gossler et al., 2019; Roshan et al., 2014). Furthermore, due to the lag of temperature change compared to water level (or hydraulic gradient) change, heat may not be an efficient tracer for rapid changes in hydraulic gradient (Constantz, 2008; Lapham, 1989).

(4) There are no constraints on applying BDFLUX to estimate sub-daily VSFs provided the temperature dataset has a sufficiently high resolution, as demonstrated by Shi et al. (2023a) and van Kampen et al. (2022). It would be a straightforward modification in the code to change the grouping of data and units for VSF estimation (e.g., from m/d to m/hour). Similar to other approaches of this type, BDFLUX obtains point estimates for a specific time, which are not necessarily representative of the surroundings or for another moment due to flux heterogeneity/temporal variability. In addition, the use of BDFLUX for estimating VSFs through temperature-time data is only feasible in the shallow subsurface or environment with concentrated groundwater fluxes (Kurylyk et al., 2019).

4. Summary and Concluding Remarks

This study presents BDFLUX, a new bounded domain model and associated MATLAB code to solve an inverse problem by analyzing on-site temperature-time series, which can be

used as a rapid- tool to quantify VSFs and thermal properties of streambed sediments. This method is based on a closed-form analytical solution that considers thermal advection and thermal conduction in a bounded (finite) streambed of interest (or streambed with layers). The VSFs, thermal properties of the streambed, and their uncertainties can be estimated simultaneously using the PSO-based parameter estimation technique and the MCMC-based parameter estimation technique. In contrast to other 1D closed-form analytical solutions, BDFLUX can handle arbitrary initial and boundary conditions based on temperature measurements at different depths within the finite streambed, and it does not assume an infinitely extending semi-infinite half space with the lower boundary condition tending towards infinity. Instead, it incorporates local top and bottom boundary conditions. Using synthetic temperature-time series, we validated the newly presented BDFLUX and demonstrated that it performs well when the top and bottom boundary conditions are determined directly by the measured data. BDFLUX also performed well in terms of interpreting laboratory experiments and field data, and the magnitude of nonvertical flow components in field of Ferencz et al. (2021) were estimated by analyzing the results of estimated VSFs in different vertical subdomains. The simulation of laboratory experiments demonstrated that the MCMC method has a lower computational efficiency than PSO method. BDFLUX can be used for assessing the magnitude of the nonvertical flow component in heterogeneous streambed sediments and is an insightful addition to current 1D closed-form analytical models.

Acknowledgments

We would like to thank the editors and two anonymous reviewers for their constructive feedback which helped to improve the article. The authors have no financial or other conflicts of interest. Data used in this manuscript were from Zhang et al. (2021) (https://zenodo.org/record/5031208) and Ferencz et al. (2021) (https://www.hydroshare.org/resource/7f0c6b909fe04efca5889fd5cd432539/). No new data were used in this manuscript. The code is available from the Hydro share data repositories: http://www.hydroshare.org/resource/1b834df0b04d4f96a4882ff00b429d42. This research was partially supported by Programs of the National Natural Science Foundation of China (grant no.42222704, grant no. 41972250 and grant no. 42272296); the Natural Science Foundation of Hubei Province (grant no.2021CFA089); Yinshanbeilu Grassland Eco-hydrology National Observation and Research Station, China Institute of Water Resources and Hydropower Research, Beijing 100038, China (grant no. YSS2022019); the National Key Research and Development Program of China (grant no. 2021YFA0715900); the 111 Program (State Administration of Foreign Experts Affairs & the Ministry of Education of China, grant no. B18049).

References

Abbott, B.W., Baranov, V.A., Mendoza Lera, C., Nikolakopoulou, M., Harjung, A., Kolbe, T., Balasubramanian, M.N., Vaessen, T.N., Ciocca, F., Campeau, A., Wallin, M.B., Romeijn, P., Antonelli, M., Gonçalves, J., Datry, T., Laverman, A.M., Dreuzy, J.-R.d., Hannah, D.M., Krause, S., Oldham, C. and Pinay, G., 2016. Using multi-tracer inference to move beyond single-catchment ecohydrology. Earth-Science Reviews, 160(2016): 19-42. https://doi.org/10.1016/j.earscirev.2016.06.014

Anderson, M.P., 2005. Heat as a ground water tracer. Ground water, 43(6): 951-68. https://doi.org/10.1111/j.1745-6584.2005.00052.x

Baek, J., Park, B.-H., Rau, G.C., Lee, K.-K., 2022. Experimental evidence for local thermal non-equilibrium during heat transport in sand representative of natural conditions. Journal of Hydrology, 608(2022): 127589. https://doi.org/10.1016/j.jhydrol.2022.127589

Banks, E.W., Shanafield, Margaret A., Noorduijn Saskia, James McCallum, Jörg Lewandowski, and Okke Batelaan, 2017. Active heat pulse sensing of 3-D-flow fields in streambeds. Hydrology and Earth System Sciences, 22(3): 1917-1929. https://doi.org/10.5194/hess-22-1917-2018

Bredehoeft, J.D., Papaopulos, I.S., 1965. Rates of vertical groundwater movement estimated from the Earth's thermal profile. Water Resources Research, 1(2): 325-328. https://doi.org/10.1029/WR001i002p00325

Chen, K., Chen, X., Song, X., Briggs, M.A., Jiang, P., Shuai, P., Hammond, G.E., Zhan, H. and Zachara, J.M., 2022a. Using ensemble data assimilation to estimate transient hydrologic exchange flow under highly dynamic flow conditions. Water Resources Research, 58(5): e2021WR030735. h. https://doi.org/10.1029/2021WR030735

Chen, K., Yin, M., Guo, Z., Liang, X., Wei, X., Yang, S., Zhai, X. and Zheng, C., 2022b. Estimating lateral groundwater inflow to rivers using heat as a tracer. Journal of Hydrology, 617(2023): 128965. https://doi.org/10.1016/j.jhydrol.2022.128965

Chen, K., Zhan, H., Wang, Q., 2018. An innovative solution of diurnal heat transport in streambeds with arbitrary initial condition and implications to the estimation of water flux and thermal diffusivity under transient condition. Journal of Hydrology, 567(2018): 361-369. https://doi.org/10.1016/j.jhydrol.2018.10.008

Conant, B., 2004. Delineating and quantifying ground water discharge zones using streambed temperatures. Ground water, 42(2): 243-57. https://doi.org/10.1111/j.1745-6584.2004.tb02671.x

Constantz, J.E., 2008. Heat as a tracer to determine streambed water exchanges. Water Resources Research, 44: W00D10. https://doi.org/10.1029/2008WR006996

De Marsily, G., 1986. Quantitative hydrogeology, Paris School of Mines, Fontainebleau.

Dya, T., Blaise, B.B., Betchewe, G., Alidou, M., 2021. Implementation of Particle Swarm Optimization Algorithm in Matlab Code for Hyperelastic Characterization. World Journal of Mechanics.

Ebbesen, S., Kiwitz, P., Guzzella, L., 2012. A generic particle swarm optimization Matlab function. 2012 American Control Conference (ACC): 1519-1524.

Ferencz, S.B., Muñoz, S., Neilson, B.T., Cardenas, M.B., 2021. Riverbed temperature and heat transport in a hydropeaked river. Water Resources Research, 57(4): e2021WR029609. https://doi.org/10.1029/2021WR029609

Ghysels, G., Anibas, C., Awol, H., Tolche, A.D., Schneidewind, U. and Huysmans, M., 2021. The significance of vertical and lateral groundwater-surface water exchange fluxes in riverbeds and riverbanks: Comparing 1D analytical flux estimates with 3D groundwater modelling. Water, 13(3): 306. https://doi.org/10.3390/w13030306

Goodman, J.R., Weare, J., 2010. Ensemble samplers with affine invariance. Communications in Applied Mathematics and Computational Science, pp. 65-80.

Gordon, R.P., Lautz, L.K., Briggs, M.A., McKenzie, J.M., 2012. Automated calculation of vertical pore-water flux from field temperature time series using the VFLUX method and computer program. Journal of Hydrology, 420(2012): 142-158. https://doi.org/10.1016/j.jhydrol.2011.11.053

Gossler, M.A., Bayer, P., Rau, G.C., Einsiedl, F., Zosseder, K., 2020. On the limitations and implications of modeling heat transport in porous aquifers by assuming local thermal equilibrium. Water Resources Research, 56(10): e2020WR027772. https://doi.org/10.1029/2020WR027772

Gossler, M.A., Bayer, P., Zosseder, K., 2019. Experimental investigation of thermal retardation and local thermal non-equilibrium effects on heat transport in highly permeable, porous aquifers. Journal of Hydrology, 578(2019): 124097. https://doi.org/10.1016/j.jhydrol.2019.124097

Goto, S., Yamano, M., Kinoshita, M., 2005. Thermal response of sediment with vertical fluid flow to periodic temperature variation at the surface. Journal of Geophysical Research, 110(B1): B01106. https://doi.org/10.1029/2004JB003419

Hatch, C.E., Fisher, A.T., Revenaugh, J.S., Constantz, J.E., Ruehl, C.R., 2006. Quantifying surface wate' groundwater interactions using time series analysis of streambed thermal records: Method development. Water Resources Research, 42(10): W10410. https://doi.org/10.1029/2005WR004787

Irvine, D.J., Briggs, M.A., Cartwright, I., Scruggs, C.R., Lautz, L.K., 2017. Improved Vertical Streambed Flux Estimation Using Multiple Diurnal Temperature Methods in Series. Ground water, 55(1): 73-80. https://doi.org/10.1111/gwat.12436

Irvine, D.J., Cartwright, I., Post, V.E.A., Simmons, C.T., Banks, E.W., 2016. Uncertainties in vertical groundwater fluxes from 1-D steady state heat transport analyses caused by heterogeneity, multidimensional flow, and climate change. Water Resources Research, 52(2): 813-826. https://doi.org/10.1002/2015WR017702

Irvine, D.J., Cranswick, R.H., Simmons, C.T., Shanafield, M.A., Lautz, L.K., 2015a. The effect of streambed heterogeneity on groundwater-surface water exchange fluxes inferred from

temperature time series. Water Resources Research, 51(1): 198-212. https://doi.org/10.1002/2014WR015769

Irvine, D.J., Kurylyk, B.L., Briggs, M.A., 2020. Quantitative guidance for efficient vertical flow measurements at the sediment-water interface using temperature-depth profiles. Hydrological Processes, 34(3): 649-661. https://doi.org/10.1002/hyp.13614

Irvine, D.J., Lautz, L.K., 2015. High resolution mapping of hyporheic fluxes using streambed temperatures: Recommendations and limitations. Journal of Hydrology, 524(2015): 137-146. https://doi.org/10.1016/j.jhydrol.2015.02.030

Irvine, D.J., Lautz, L.K., Briggs, M.A., Gordon, R.P., McKenzie, J.M., 2015b. Experimental evaluation of the applicability of phase, amplitude, and combined methods to determine water flux and thermal diffusivity from temperature time series using VFLUX 2. Journal of Hydrology, 531(3): 728-737. https://doi.org/10.1016/j.jhydrol.2015.10.054

van Kampen, R., Schneidewind, U., Anibas, C., Bertagnoli, A., Tonina, D., Vandersteen, G., Luce, C.H., Krause, S. and Berkel, M.V., 2022. LPMLE n- A frequency domain method to estimate vertical streambed fluxes and sediment thermal properties in semi-infinite and bounded domains. Water Resources Research, 58(3): e2021WR030886. https://doi.org/10.1029/2021WR030886

Keery, J., Binley, A., Crook, N., Smith, J.W.N., 2007. Temporal and spatial variability of groundwater surface water fluxes: Development and application of an analytical method using temperature time series. Journal of Hydrology, 336(1-2): 1-16. https://doi.org/10.1016/j.jhydrol.2006.12.003

Klepikova, M.V., Wildemeersch, S., Hermans, T., Jamin, P., Orban, P., Nguyen, F., Brouyère, S. and Dassargues, A., 2016. Heat tracer test in an alluvial aquifer: Field experiment and inverse modelling. Journal of Hydrology, 540(2016): 812-823. https://doi.org/10.1016/j.jhydrol.2016.06.066

Krause, S., Abbott, B.W., Baranov, V.A., Bernal, S., Blaen, P.J., Datry, T., Drummond, J.D., Fleckenstein, J.H., Velez, J.G., Hannah, D.M., Knapp, J.L.A., Kurz, M.J., Lewandowski, J., Martí, E., Mendoza‐Lera, C., Milner, A.M., Packman, A.I., Pinay, G., Ward, A.S. and Zarnetzke, J.P., 2022. Organizational principles of hyporheic exchange flow and biogeochemical cycling in river networks across scales. Water Resources Research, 58(3): e2021WR029771. https://doi.org/10.1029/2021WR029771

Kurylyk, B.L., MacQuarrie, K.T.B., 2014. A new analytical solution for assessing climate change impacts on subsurface temperature. Hydrological Processes, 28(7): 3161-3172. https://doi.org/10.1002/hyp.9861

Kurylyk, B.L., Irvine, D.J., 2016. Analytical solution and computer program (FAST) to estimate fluid fluxes from subsurface temperature profiles. Water Resources Research, 52(2): 725-733. https://doi.org/10.1002/2015WR017990

Kurylyk, B.L., Irvine, D.J., Carey, S.K., Briggs, M.A., Werkema, D.D. and Bonham, M., 2017. Heat as a groundwater tracer in shallow and deep heterogeneous media: Analytical solution, spreadsheet tool, and field applications. Hydrological Processes, 31(14): 2648 2661. https://doi.org/10.1002/hyp.11216

Kurylyk, B.L., Irvine, D.J., Bense, V.F., 2019. Theory, tools, and multidisciplinary applications for tracing groundwater fluxes from temperature profiles. Wires Water, 6(1): e1329. https://doi.org/10.1002/wat2.1329

Lapham, W.W., 1989. Use of temperature profiles beneath streams to determine rates of vertical ground-water flow and vertical hydraulic conductivity. Dept. of the Interior, U.S. Geological Survey ; U.S. G.P.O. ; Books and Open- File Reports Section, U.S. Geological Survey. https://doi.org/10.3133/wsp2337

Lautz, L.K., 2010. Impacts of nonideal field conditions on vertical water velocity estimates from streambed temperature time series. Water Resources Research, 46(1): W01509. https://doi.org/10.1029/2009WR007917

Leij, F.J., Priesack, E., Schaap, M.G., 2000. Solute transport modeled with Green's functions with application to persistent solute sources. Journal of Contaminant Hydrology, 41(2000): 155-173. https://doi.org/10.1016/S0169-7722(99)00062-5Liang, X., Zhang, Y.K., Liu, J., Ma, E., Zheng, C., 2019. Solute Transport With Linear Reactions in Porous Media With Layered Structure: A Semianalytical Model. Water Resources Research, 55(6): 5102 - 5118. https://doi.org/10.1029/2019WR024778

Lin, Y., Chang, C., Tsai, J., 2022. Analytical solution for estimating transient vertical groundwater flux from temperature-depth profiles. Journal of Hydrology, 610(2022): 127920. https://doi.org/10.1016/j.jhydrol.2022.127920

Lu, N., Ge, S., 1996. Effect of horizontal heat and fluid flow on the vertical temperature distribution in a semiconfining layer. Water Resources Research, 32(5): 1449-1453. https://doi.org/10.1029/95WR03095

Luce, C.H., Tonina, D., Applebee, R.C., DeWeese, T., 2017. Was That Assumption Necessary? Reconsidering Boundary Conditions for Analytical Solutions to Estimate Streambed Fluxes. Water Resources Research, 53(11): 9771-9790. https://doi.org/10.1002/2017WR020618

Luce, C.H., Tonina, D., Gariglio, F., Applebee, R.C., 2013. Solutions for the diurnally forced advection diffusion equation to estimate bulk fluid velocity and diffusivity in streambeds from temperature time series. Water Resources Research, 49(1): 488-506. https://doi.org/10.1029/2012WR012380

McCallum, A.M., Andersen, M.S., Rau, G.C., Acworth, R., 2012. A 1-D analytical method for estimating surface water-groundwater interactions and effective thermal diffusivity using temperature time series. Water Resources Research, 48(11): W11532. https://doi.org/10.1029/2012WR012007

Munz, M., Oswald, S.E., Schmidt, C., 2016. Analysis of riverbed temperatures to determine the geometry of subsurface water flow around in-stream geomorphological structures. Journal of Hydrology, 539(2016): 74-87. https://doi.org/10.1016/j.jhydrol.2016.05.012

Pallero, J.L.G. et al., 2018. Particle Swarm Optimization and Uncertainty Assessment in Inverse Problems. Entropy, 20(2): 96. https://doi.org/10.3390/e20020096

Rau, G.C., Andersen, M.S., McCallum, A.M., Acworth, R., 2010. Analytical methods that use natural heat as a tracer to quantify surface water–groundwater exchange, evaluated using field temperature records. Hydrogeology Journal, 18(2010): 1093-1110. https://doi.org/10.1007/s10040-010-0586-0

Rau, G.C., Andersen, M.S., Acworth, R., 2012. Experimental investigation of the thermal dispersivity term and its significance in the heat transport equation for flow in sediments. Water Resources Research, 48(3): W03511. https://doi.org/10.1029/2011WR011038

Rau, G.C., Andersen, M.S., McCallum, A.M., Roshan, H., Acworth, R., 2014. Heat as a tracer to quantify water flow in near-surface sediments. Earth-Science Reviews, 129(2014): 40-58. https://doi.org/10.1016/j.earscirev.2013.10.015

Reeves, J.M., Hatch, C.E., 2016. Impacts of three- dimensional nonuniform flow on quantification of groundwater surface water interactions using heat as a tracer. Water Resources Research, 52(9): 6851-6866. https://doi.org/10.1002/2016WR018841

Ren, J., Cheng, J., Yang, J., Zhou, Y.-j., 2018. A review on using heat as a tool for studying groundwater-surface water interactions. Environmental Earth Sciences, 77(22): 1-13. https://doi.org/10.1007/s12665-018-7959-4

Ronan, A.D., Prudic, D.E., Thodal, C.E., Constantz, J.E., 1998. Field study and simulation of diurnal temperature effects on infiltration and variably saturated flow beneath an ephemeral stream. Water Resources Research, 34(9): 2137-2153. https://doi.org/10.1029/98WR01572

Roshan, H., Cuthbert, M.O., Cuthbert, M.O., Andersen, M.S., Acworth, R., 2014. Local thermal non-equilibrium in sediments: Implications for temperature dynamics and the use of heat as a tracer. Advances in Water Resources, 73(2014): 176-184. https://doi.org/10.1016/j.advwatres.2014.08.002

Saar, M.O., 2011. Review: Geothermal heat as a tracer of large-scale groundwater flow and as a means to determine permeability fields. Hydrogeology Journal, 19: 31-52. https://doi.org/10.1007/s10040-010-0657-2

Schneidewind, U., Berkel, M.v., Anibas, C., Vandersteen, G., Schmidt, C., Joris, I., Seuntjens, P., Batelaan, O. and Zwart, H.J., 2016. LPMLE3: A novel 1-D approach to study water flow in streambeds using heat as a tracer. Water Resources Research, 52(8): 6596-6610. https://doi.org/10.1002/2015WR017453

Selker, J.S., Thévenaz, L., Huwald, H., Mallet, A., Luxemburg, W., Giesen, N.v.d., Stejskal, M., Zeman, J., Westhoff, M. and Parlange, M.B., 2006. Distributed fiber-optic temperature

sensing for hydrologic systems. Water Resources Research, 42: W12202. https://doi.org/10.1029/2006WR005326

Shi, W., Wang, Q., 2023. An analytical model of multi-layered heat transport to estimate vertical streambed fluxes and sediment thermal properties. Journal of Hydrology, 625(2023): 129963. https://doi.org/10.1016/j.jhydrol.2023.129963

Shi, W., Zhan, H., and Wang, Q., 2023a. Quantifying vertical streambed fluxes and streambed thermal properties using heat as a tracer during extreme hydrologic events. Journal of Hydrology, 629(2024): 130553. https://doi.org/10.1016/j.jhydrol.2023.130553

Shi, W., Zhan, H., Wang, Q., Xie, X., 2023b. A two‐dimensional closed‐form analytical solution for heat transport with nonvertical flow in riparian zones. Water Resources Research, 59(8): e2022WR034059. https://doi.org/10.1029/2022WR034059.

Stallman, 1965. Steady one-dimensional fluid flow in a sem-infinite porous medium with sinusoidal surface temperature. Journal of Geophysical Research, 70(12): 2821-2827. https://doi.org/10.1029/JZ070i012p02821

Stonestrom, D.A., Constantz, J.E., 2003. Heat as a tool for studying the movement of ground water near streams. Circular. US Department of the Interior, US Geological Survey. https://doi.org/10.3133/cir1260

Suzuki, S., 1960. Percolation measurements based on heat flow through soil with special reference to paddy fields. Journal of Geophysical Research, 65(9): 2883-2885. https://doi.org/10.1029/JZ065i009p02883

Taniguchi, M., Shimada, J., Tanaka, T., Kayane, I., Sakura, Y., Shimano, Y., Dapaah-Siakwan, S. and Kawashima, S., 1999. Disturbances of temperature-depth profiles due to surface climate change and subsurface water flow: 1. An effect of linear increase in surface temperature caused by global warming and urbanization in the Tokyo Metropolitan Area, Japan. Water Resources Research, 35(5): 1507-1517. https://doi.org/10.1029/1999WR900009

Tripathi, M., Yadav, P.K., Chahar, B.R., Dietrich, P., 2021. A review on groundwater surface water interaction highlighting the significance of streambed and aquifer properties on the exchanging flux. Environmental Earth Sciences, 80: 1-16. https://doi.org/10.1007/s12665-021-09897-9

Vandersteen, G., Schneidewind, U., Anibas, C., Schmidt, C., Seuntjens, P. and Batelaan, O., 2015. Determining groundwater surface water exchange from temperature-time series: Combining a local polynomial method with a maximum likelihood estimator. Water Resources Research, 51(2): 922-939. https://doi.org/10.1002/2014WR015994

Vogt, T., Schneider, P., Hahn-Woernle, L., Cirpka, O.A., 2010. Estimation of seepage rates in a losing stream by means of fiber-optic high-resolution vertical temperature profiling. Journal of Hydrology, 380(1-2): 154-164. https://doi.org/10.1016/j.jhydrol.2009.10.033

Zhang, J., Man, J., Lin, G., Wu, L., Zeng, L., 2017. Inverse modeling of hydrologic systems with adaptive multi-fidelity Markov chain Monte Carlo simulations. Water Resources Research, 54(7): 4867 - 4886. https://doi.org/10.1029/2018WR022658

Zhang, Y., Yu, X., Fleckenstein, J.H., Sun, H., Lu, C., Yin, M., Ma, R., Salsky, K., Wei, W. and Zheng, C., 2021. Upscaling Heat Flow in Porous Media With Periodic Surface Temperature Fluctuation Using a One-Dimensional Subordinated Heat Transfer Equation. Water Resources Research, 57(7): e2020WR027266. https://doi.org/10.1029/2020WR027266

Figure Captions:

Figure 1. Flow chart of proposed conceptual model with the three steps for parameter estimation: (a). Conceptual model and its analytical solution; (b). Collected temperature-time series in the streambed at different depths, data from Ferencz et al. (2021); (c). Parameter estimation using particle swarm optimization (PSO) and Markov Chain Monte Carlo (MCMC) techniques.

Figure 2. (a) Schematic diagram for the laboratory experimental system; (b) - (d) are temperature-time series observed at $z = 0.0$, 0.1 and 0.2 m, respectively, where (b) and (d) serve as top and bottom boundary conditions of the BDFLUX model, and (c) is used for parameter estimation. These observed data are from the experiment Run1 of Zhang et al. (2021).

Figure 3. Comparison of temperature-time series between BDFLUX (black solid curves) and numerical solution (green circle symbols) at $z = 0.1$, 0.2 and 0.3 m, respectively. The top and bottom boundary conditions are from Ferencz et al. (2021), as shown in Figure 1b, where "BS1" and "OBS3" serve as top and bottom boundary conditions, respectively.

Figure 4. Comparison of temperature-time series predicted by the BDFLUX (solid curves) and semi-infinite domain model (dashed curves) at $z = 0.1$, 0.2 and 0.3 m. (a) $q = 0.01$ m/d, (b) $q = 0.10$ m/d, (c) $q = 0.50$ m/d. "BC" in the legend represents boundary condition, "BDM" and "SIM" refer to bounded domain model and semi-infinite domain model, respectively.

Figure 5. Simulation results of the laboratory experiments of Run1 (a) and Run2 (b) at $z = 0.1$ m: The observed data (green circle symbols) versus the BDFLUX (red solid curves) and the models of Zhang et al. (2021).

Figure 6. Simulation results of the laboratory experiment of Run1 using MCMC method. The results of PSO method (Red solid curve) and the Sub-HTE model of Zhang et al. (2021) (Magenta solid curve) are also included for comparison. The frequency histograms of the thermal front velocity (a) and the effective thermal diffusivity (b) estimated by the MCMC method. (c) Comparison between the measured data and predicted temperature-time series, where the blue solid curve generated by BDFLUX based on the parameter samples from MCMC.

Figure 7. Simulation results of the laboratory experiment of Run2 using MCMC method. The results of PSO method (Red solid curve) and the Sub-HTE model of Zhang et al. (2021)

(Magenta solid curve) are also included for comparison. The frequency histograms of the thermal front velocity (a) and the effective thermal diffusivity (b) estimated by the MCMC method. (c) Comparison between the measured data and predicted temperature-time series, where the blue solid curve generated by BDFLUX based on the parameter samples from MCMC.

Figure 8. Fitting of the temperature-time series (green circle symbols) observed at VA1 by the BDFLUX (red solid curves) using the estimated parameters obtained from the PSO method for (a) SDI, (b) SDII, and (c) SDIII. The top and bottom boundary conditions of the BDFLUX are represented by the blue and black solid curves. Data from Ferencz et al. (2021).

Figure 9. Fitting of the temperature-time series (green circle symbols) observed at VA2 by BDFLUX (red solid curves) using the estimated parameters obtained from the PSO method for (a) SDI, (b) SDII, and (c) SDIII. The top and bottom boundary conditions of BDFLUX are represented by the blue and black solid curves. Data from Ferencz et al. (2021).

Figure 10. The estimated VSFs and the inferred magnitude of nonvertical flow components in streambed profile VA1 (a)and streambed profile VA2 (b). Differences in VSFs between SDI and SDII imply a change in the magnitude of the nonvertical flow component (magenta arrow). The unit of VSFs are in $\mathrm{m/d}$.

Table Captions

Table 1. The values of D and v are used as true values in the numerical model (NUM) and are estimated by BDFLUX, and the relative error between true and estimated values are calculated. The generated temperature-time series at the depths of 0.1, 0.2 and 0.3 m are used to estimate D and v by BDFLUX.

Table 2. Parameters estimated by different models using laboratory experimental data

Table 3. Estimated thermal conductivity and volumetric heat capacity using different models.

Journal Pre-proofs

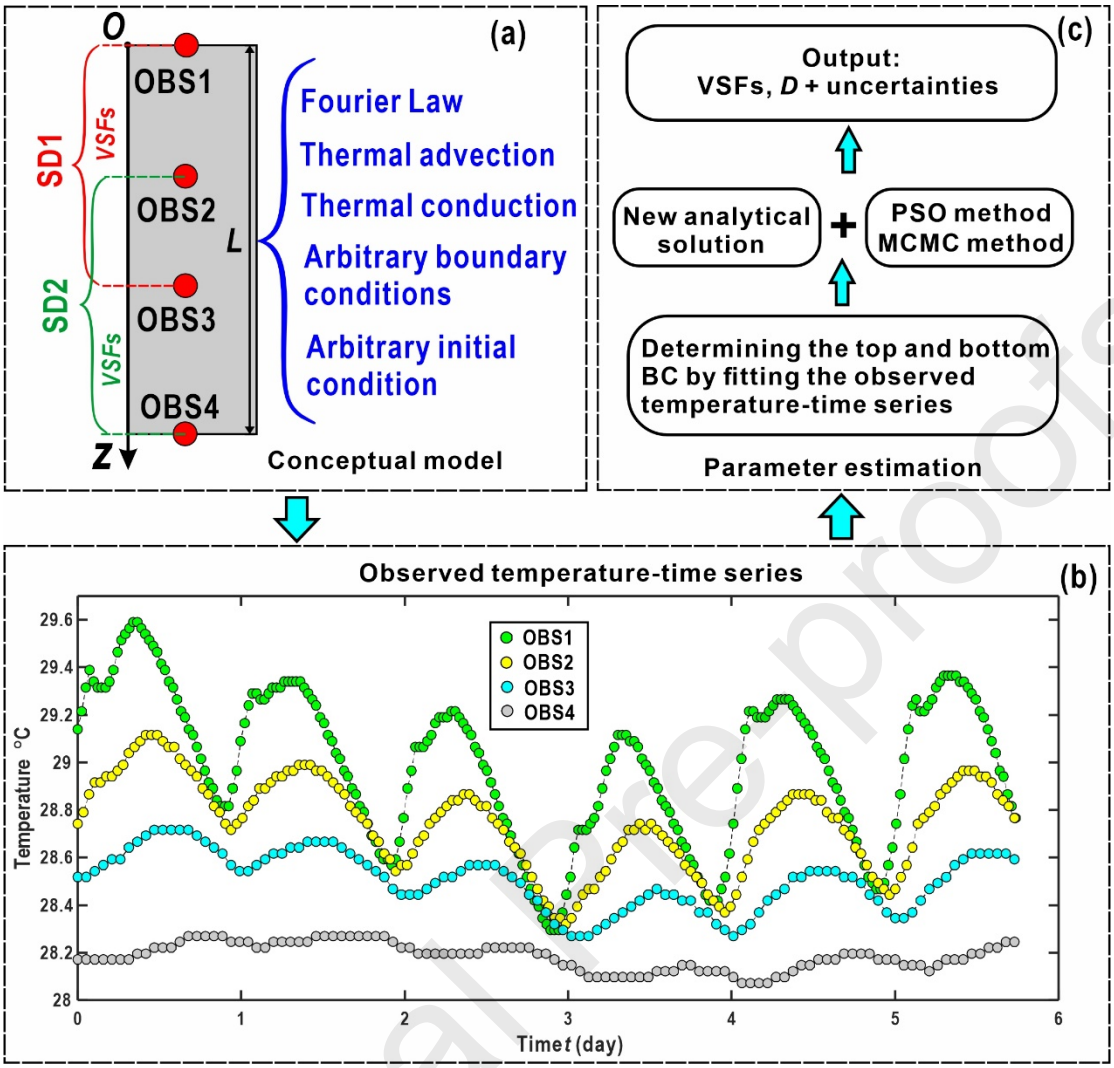

867

868 **Figure 1.** Flow chart of proposed conceptual model with the three steps for parameter
869 estimation: (a). Conceptual model and its analytical solution; (b). Collected temperature-time
870 series in the streambed at different depths, data from Ferencz et al. (2021); (c). Parameter
871 estimation using particle swarm optimization (PSO) and Markov Chain Monte Carlo (MCMC)
872 techniques.

873

Journal Pre-proofs

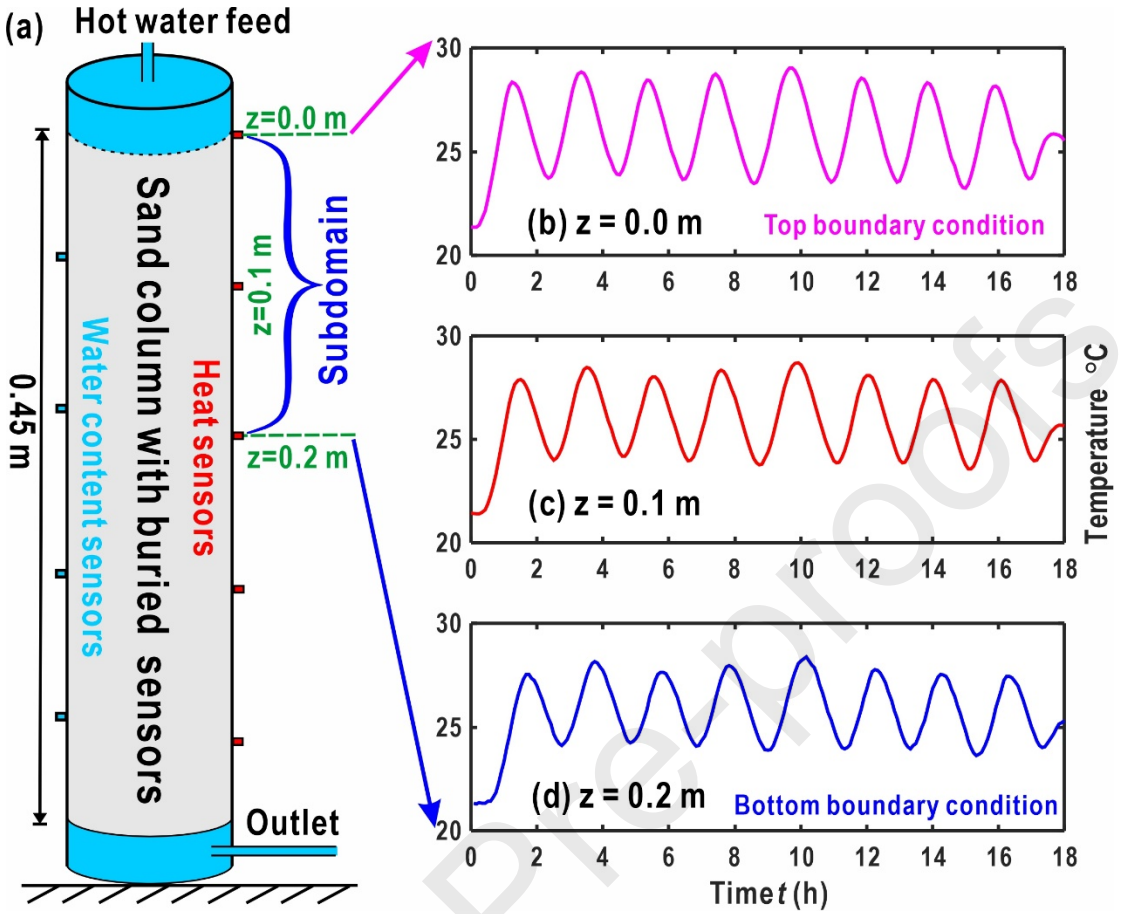

874

875 **Figure 2.** (a) Schematic diagram for the laboratory experimental system; (b) - (d) are
876 temperature-time series observed at $z = 0.0$, 0.1 and 0.2 m, respectively, where (b) and (d) serve
877 as top and bottom boundary conditions of the BDFLUX model, and (c) is used for parameter
878 estimation. These observed data are from the experiment Run1 of Zhang et al. (2021).

879

Journal Pre-proofs

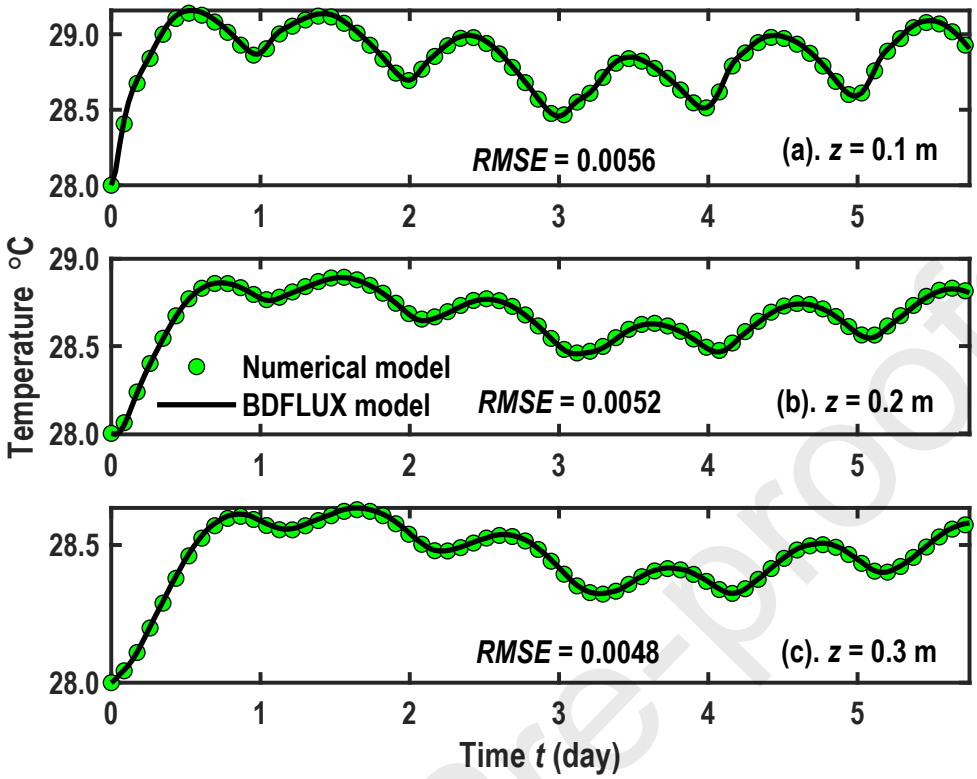

Figure 3. Comparison of temperature-time series between BDFLUX (black solid curves) and numerical solution (green circle symbols) at $z = 0.1$, 0.2 and 0.3 m, respectively. The top and bottom boundary conditions are from Ferencz et al. (2021), as shown in Figure 1b, where "BS1" and "OBS3" serve as top and bottom boundary conditions, respectively.

Journal Pre-proofs

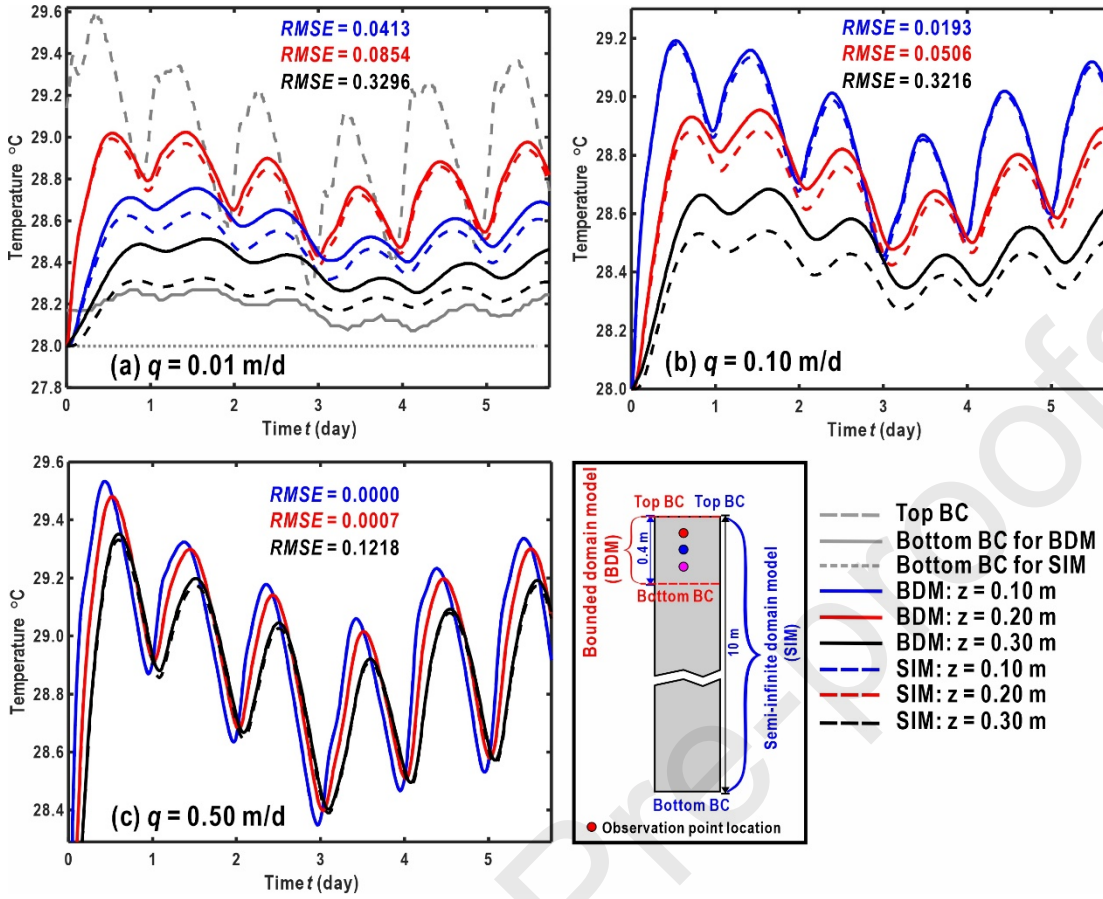

885

886 **Figure 4.** Comparison of temperature-time series predicted by the BDFLUX (solid curves) and
887 semi-infinite domain model (dashed curves) at $z = 0.1$, 0.2 and 0.3 m. (a) $q = 0.01$ m/d, (b)
888 $q = 0.10$ m/d, (c) $q = 0.50$ m/d. "BC" in the legend represents boundary condition, "BDM"
889 and "SIM" refer to bounded domain model and semi-infinite domain model, respectively.

890

Journal Pre-proofs

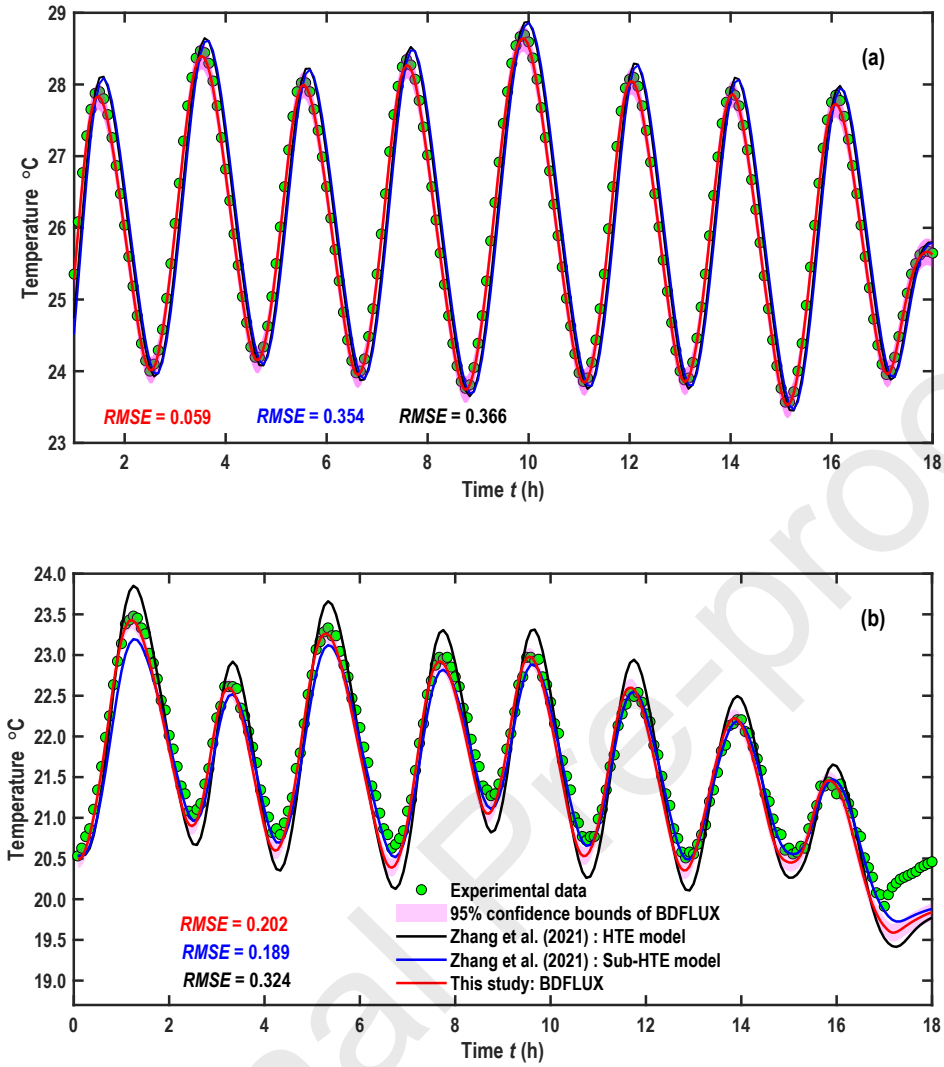

Figure 5. Simulation results of the laboratory experiments of Run1 (a) and Run2 (b) at $z = 0.1$ m: The observed data (green circle symbols) versus the BDFLUX (red solid curves) and the models of Zhang et al. (2021).

Journal Pre-proofs

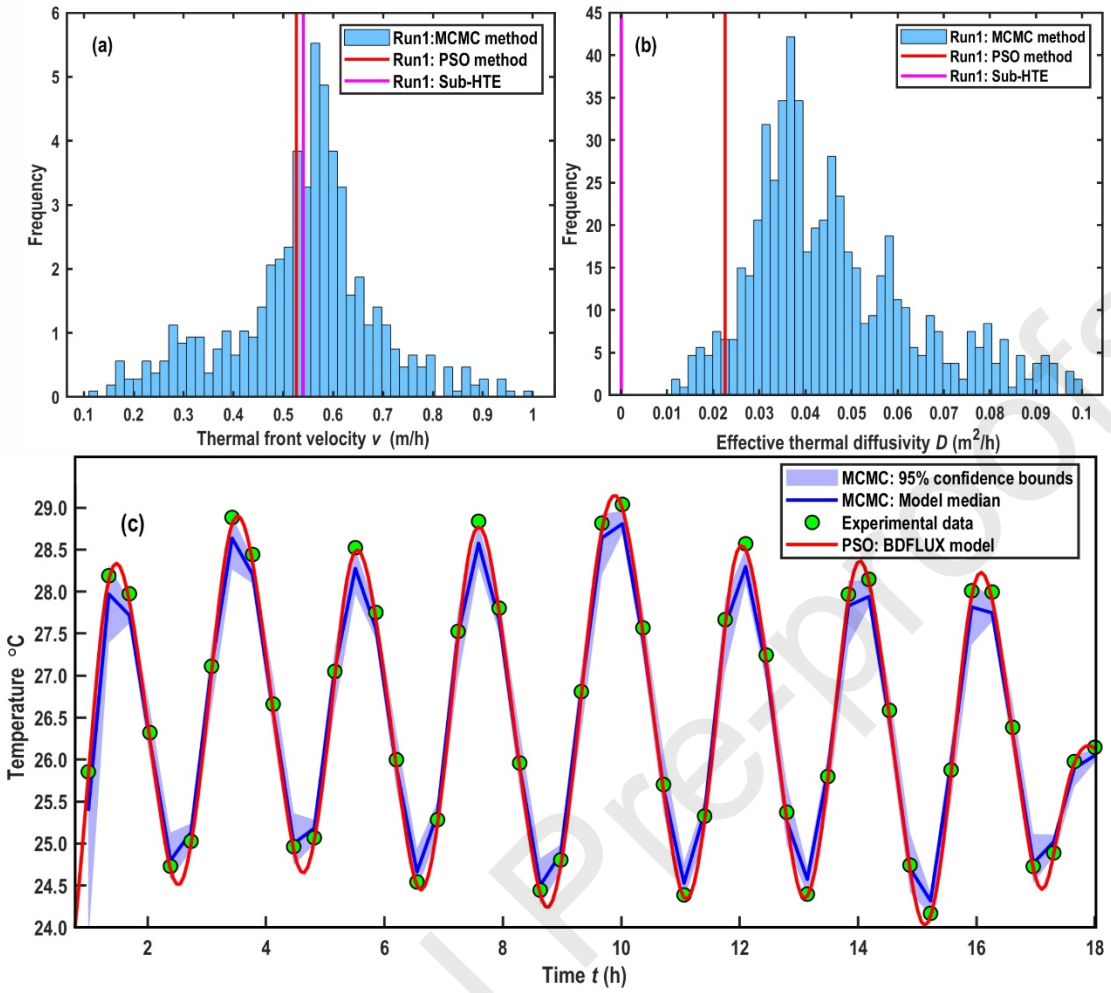

Figure 6. Simulation results of the laboratory experiment of Run1 using MCMC method. The results of PSO method (Red solid curve) and the Sub-HTE model of Zhang et al. (2021) (Magenta solid curve) are also included for comparison. The frequency histograms of the thermal front velocity (a) and the effective thermal diffusivity (b) estimated by the MCMC method. (c) Comparison between the measured data and predicted temperature-time series, where the blue solid curve generated by BDFLUX based on the parameter samples from MCMC.

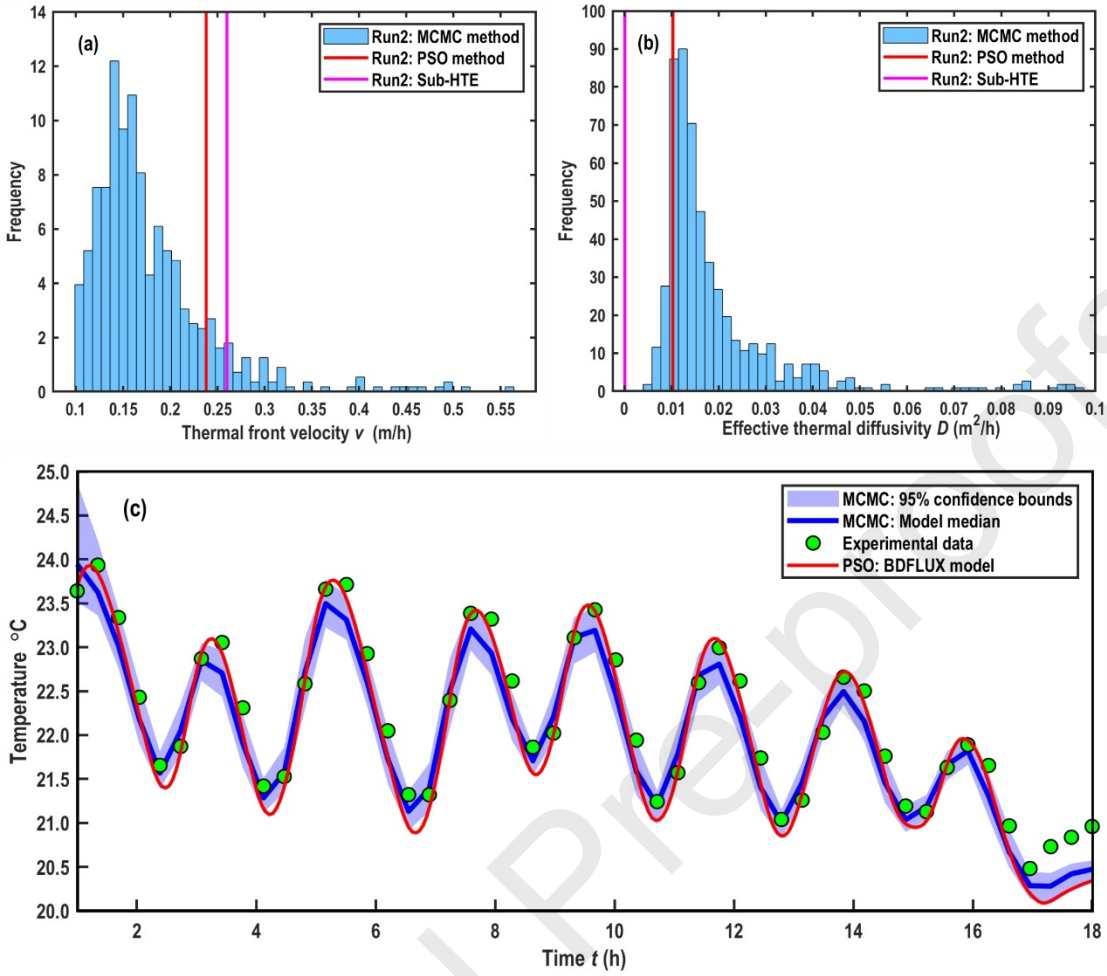

903

904 **Figure 7.** Simulation results of the laboratory experiment of Run2 using MCMC method. The
905 results of PSO method (Red solid curve) and the Sub-HTE model of Zhang et al. (2021)
906 (Magenta solid curve) are also included for comparison. The frequency histograms of the thermal
907 front velocity (a) and the effective thermal diffusivity (b) estimated by the MCMC method. (c)
908 Comparison between the measured data and predicted temperature-time series, where the blue
909 solid curve generated by BDFLUX based on the parameter samples from MCMC.

Journal Pre-proofs

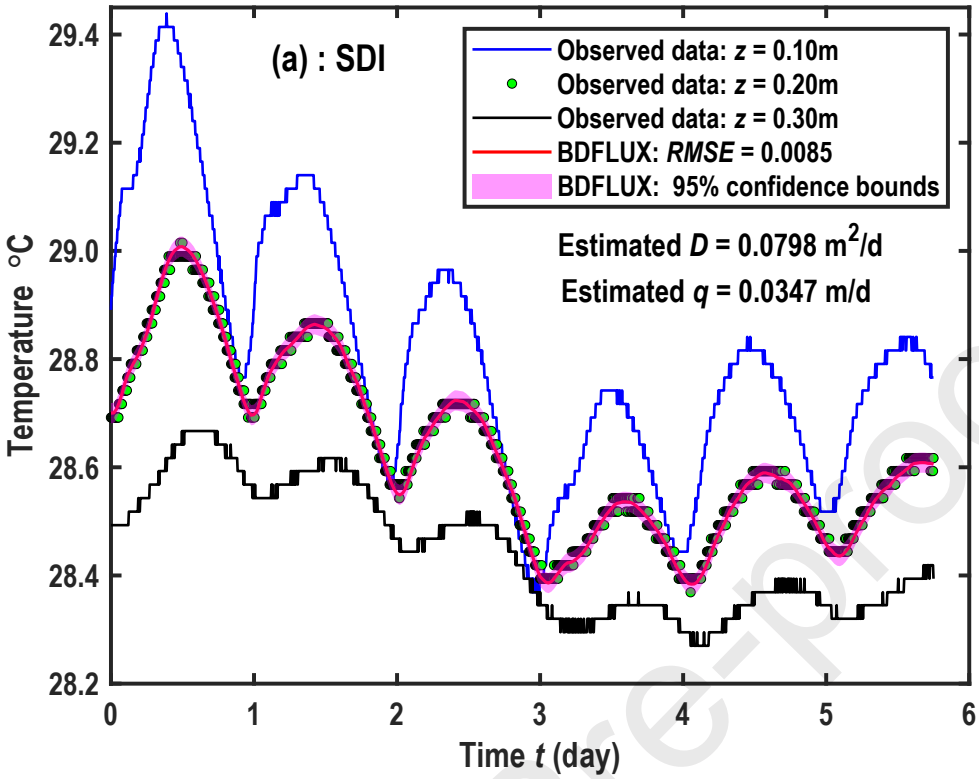
(a) : SDI
Observed data: z = 0.10m
Observed data: z = 0.20m
Observed data: z = 0.30m
BDFLUX: RMSE = 0.0085
BDFLUX: 95% confidence bounds
Estimated D = 0.0798 m2/d
Estimated q = 0.0347 m/d
Temperature °C
Time t (day)
29.4
29.2
29.0
28.8
28.6
28.4
28.2
0
1
2
3
4
5
6

910

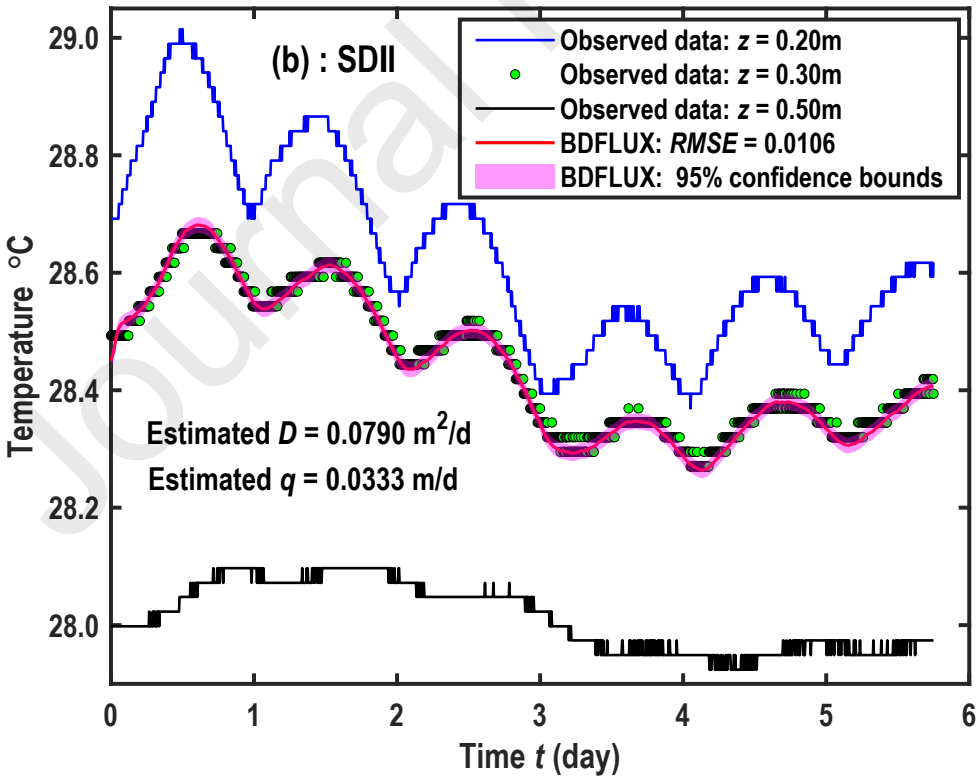
(b) : SDII
Observed data: z = 0.20m
Observed data: z = 0.30m
Observed data: z = 0.50m
BDFLUX: RMSE = 0.0106
BDFLUX: 95% confidence bounds
Estimated D = 0.0790 m2/d
Estimated q = 0.0333 m/d
Temperature °C
Time t (day)
29.0
28.8
28.6
28.4
28.2
28.0
0
1
2
3
4
5
6

911

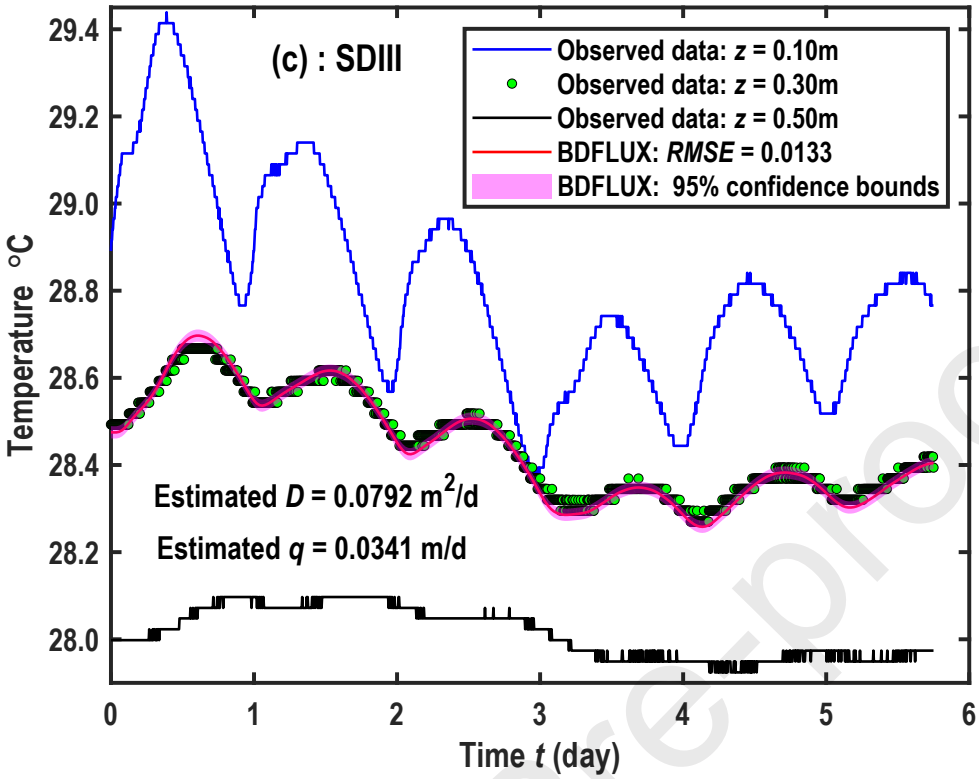

912

913 **Figure 8.** Fitting of the temperature-time series (green circle symbols) observed at VA1 by the
914 BDFLUX (red solid curves) using the estimated parameters obtained from the PSO method for
915 (a) SDI, (b) SDII and (c) SDIII. The top and bottom boundary conditions of the BDFLUX are
916 represented by the blue and black solid curves. Data are from Ferencz et al. (2021).

917

Journal Pre-proofs

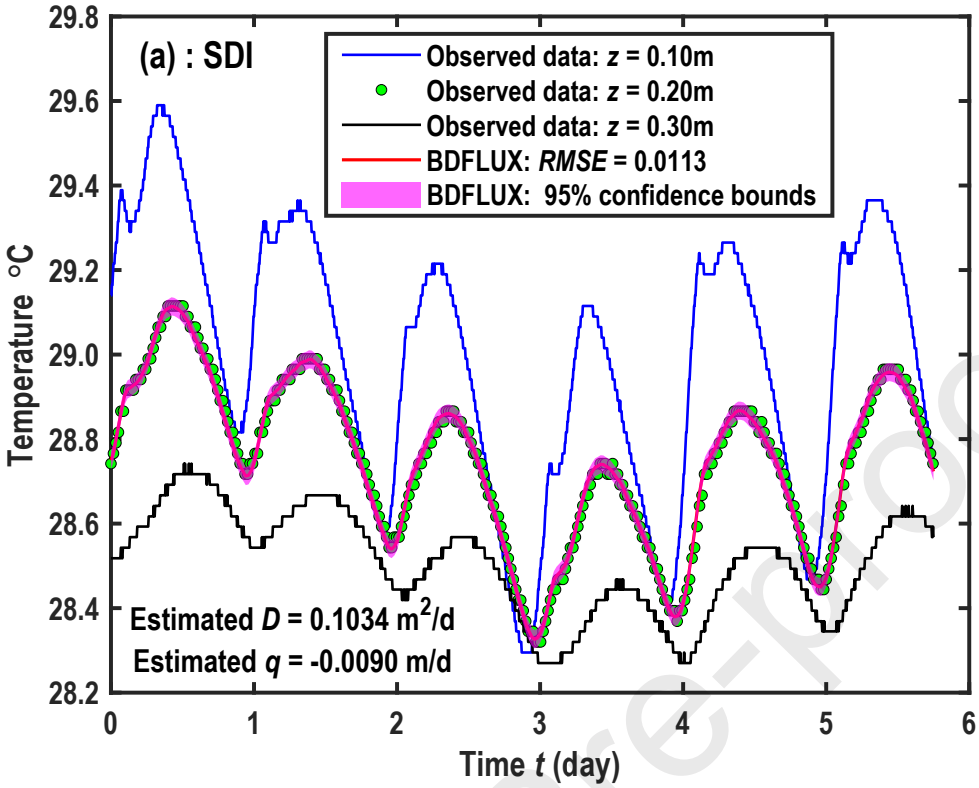
(a) : SDI
Observed data: z = 0.10m
Observed data: z = 0.20m
Observed data: z = 0.30m
BDFLUX: RMSE = 0.0113
BDFLUX: 95% confidence bounds
Estimated D = 0.1034 m2/d
Estimated q = -0.0090 m/d
Temperature °C
Time t (day)

918

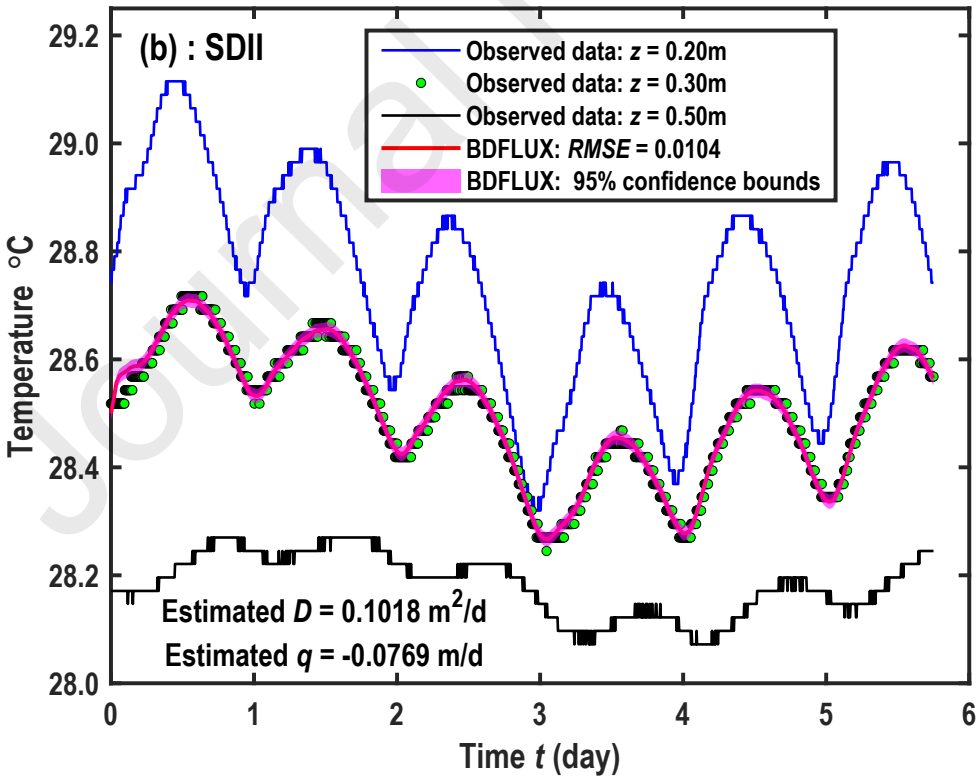
(b) : SDII
Observed data: z = 0.20m
Observed data: z = 0.30m
Observed data: z = 0.50m
BDFLUX: RMSE = 0.0104
BDFLUX: 95% confidence bounds
Estimated D = 0.1018 m2/d
Estimated q = -0.0769 m/d
Temperature °C
Time t (day)

919

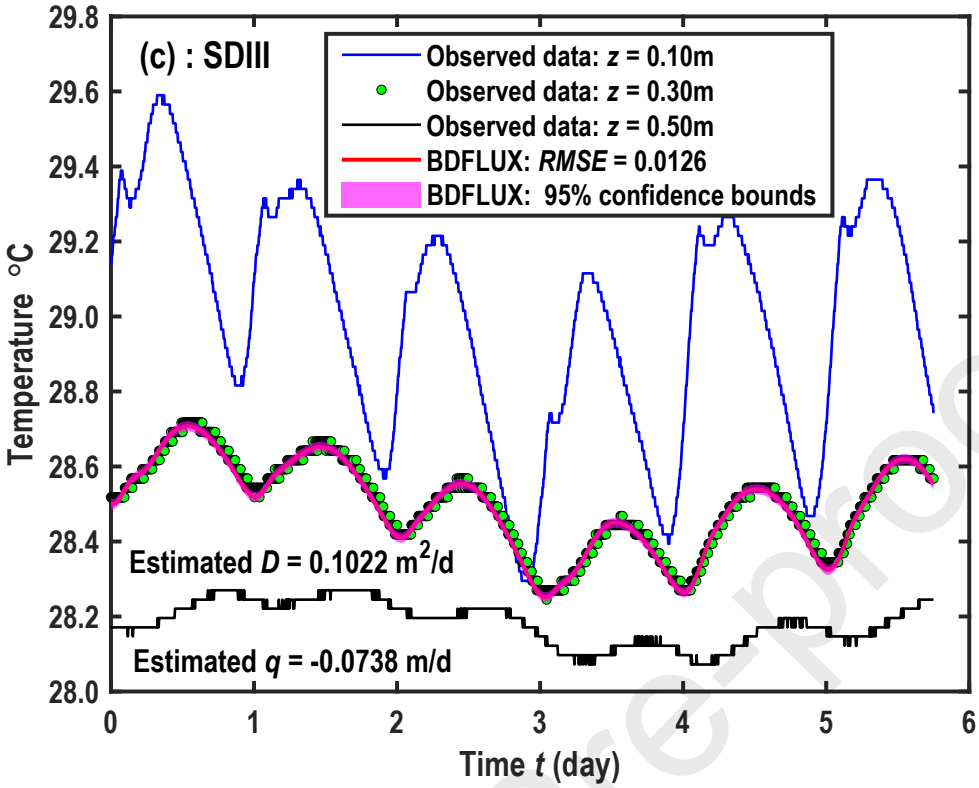

Figure 9. Fitting of the temperature-time series (green circle symbols) observed at VA2 by BDFLUX (red solid curves) using the estimated parameters obtained from the PSO method for (a) SDI, (b) SDII and (c) SDIII. The top and bottom boundary conditions of BDFLUX are represented by the blue and black solid curves. Data are from Ferencz et al. (2021).

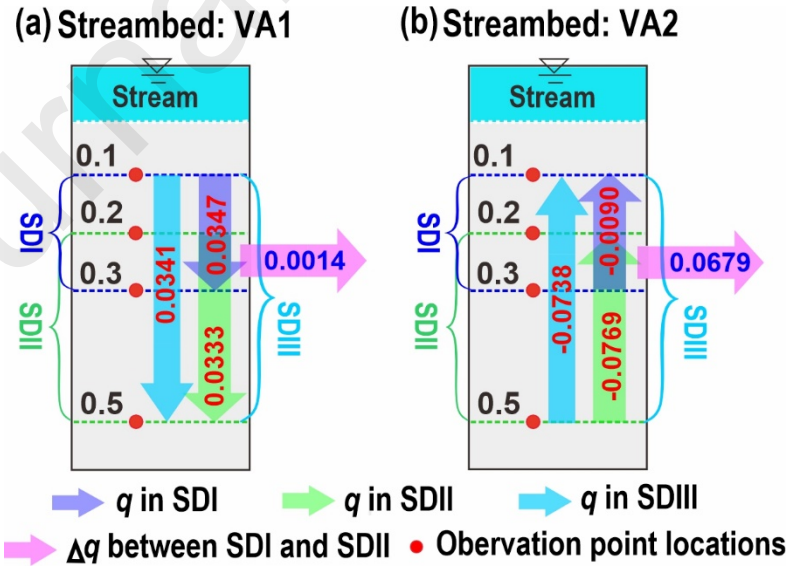

Figure 10. The estimated VSFs and the inferred magnitude of nonvertical flow components in streambed profile VA1 (a)and streambed profile VA2 (b). Differences in VSFs between SDI and

928 SDII imply a change in the magnitude of the nonvertical flow component (magenta arrow). The
929 unit of VSFs are in $\mathrm{m/d}$.

930

931 **Table 1.** The values of D and v are used as true values in the numerical model (NUM) and are
932 estimated by BDFLUX, and the relative error between true and estimated values are calculated. The
933 generated temperature-time series at the depths of 0.1, 0.2 and 0.3 m are used to estimate D and v by
934 BDFLUX.

Scenarios	Parameters	True values	Estimated value by BDFLUX	Relative error (%)
$q = 0.01$ [m/d]	D [$\mathrm{m^2/d}$]	0.0491	0.0479	2.44
	v [m/d]	0.0231	0.0238	3.03
$q = 0.10$ [m/d]	D [$\mathrm{m^2/d}$]	0.0491	0.0475	3.25
	v [m/d]	0.2308	0.2340	1.39
$q = 0.50$ [m/d]	D [$\mathrm{m^2/d}$]	0.0491	0.0469	4.07
	v [m/d]	1.1538	1.1781	2.11

935 The other parameters used to calculate D and v are: $k = 1.44\ \mathrm{W/(m \cdot K)}$, $\rho c = 2.534 \times 10^6\ \mathrm{J/(m^3 \cdot K)}$, and $\rho_w c_w = 4.20 \times 10^6\ \mathrm{J/(m^3 \cdot K)}$.

937

938 **Table 2.** Parameters estimated by different models using laboratory experimental data

Tests	Parameters	Symbols	Models		
			BDFLUX	Sub-HTE[a]	HTE[a]
Run1	Best-fit effective thermal diffusivity	D [$\mathrm{m^2/h}$]	0.0226	0.0001	0.0004

Journal Pre-proofs

	Best-fit thermal front velocity	v [m/h]	0.5261	0.5400	0.5800
	Best-fit fractional order [a]	α [-]	N/A	0.90	N/A
	Root mean square error	$RMSE$ [-]	0.0590	0.3540	0.3660
	Best-fit effective thermal diffusivity	D [m^2/h]	0.0103	0.0001	0.0004
	Best-fit thermal front velocity	v [m/h]	0.2380	0.2600	0.3200
Run2	Best-fit fractional order [a]	α [-]	N/A	0.78	N/A
	Root mean square error	$RMSE$ [-]	0.202	0.189	0.324

[a]. The models and parameter values are from Zhang et al. (2021).

Table 3. Estimated thermal conductivity and volumetric heat capacity using different models.

Tests	Models	Estimated parameters					
		θ [-]	k_s [W/(m · K)]	$\rho_s c_s$ [J/(m^3 · K)]	β [m]	D [m^2/h]	v [m/h]
Run1	Sub-THE model	0.45	-0.357	1.527×10^6	N/A	0.0001	0.5400
	HTE model	0.45	0.022	1.182×10^6	N/A	0.0004	0.5800
	BDFLUX with β	0.4514	9.820	1.652×10^6	0.0291	0.0226	0.5261

	BDFLUX without β	0.2093	22.071	2.432×10^6	N/A	0.0226	0.5261
Run2	Sub-THE model	0.45	-0.329	2.400×10^6	N/A	0.0001	0.2600
	HTE model	0.45	0.036	1.291×10^6	N/A	0.0004	0.3200
	BDFLUX with β	0.3856	9.069	3.192×10^6	0.0181	0.0101	0.2334
	BDFLUX without β	0.1898	12.439	3.386×10^6	N/A	0.0104	0.2361

Highlights

- Heat-based bounded domain analytical model for vertical streambed flux presented.
- Particle swarm optimization and Markov Chain Monte Carlo methods used.
- Model is evaluated using synthetic, laboratory experimental, and field data.
- Method to estimate nonvertical flow components presented.

Declaration of interests

☒ The authors declare that they have no known competing financial interests or personal relationships that could have appeared to influence the work reported in this paper.

☐The authors declare the following financial interests/personal relationships which may be considered as potential competing interests:

Journal Pre-proofs

Declaration of interests

☒ The authors declare that they have no known competing financial interests or personal relationships that could have appeared to influence the work reported in this paper.

☐The authors declare the following financial interests/personal relationships which may be considered as potential competing interests:

Journal Pre-proofs